Coresets from Trajectories: Selecting Data via Correlation of Loss Differences

Anonymous authors
Paper under double-blind review

Abstract

Deep learning models achieve state-of-the-art performance across domains but face scalability challenges in real-time or resource-constrained scenarios. To address this, we propose *Correlation of Loss Differences* (`CLD`), a simple and scalable metric for coreset selection that identifies the most impactful training samples by measuring their alignment with the loss trajectories of a held-out validation set. `CLD` is highly efficient, requiring only per-sample loss values computed at training checkpoints, and avoiding the costly gradient and curvature computations used in many existing subset selection methods. We develop a general theoretical framework that establishes convergence guarantees for `CLD`-based coresets, demonstrating that the convergence error is upper-bounded by the alignment of the selected samples and the representativeness of the validation set. On CIFAR-100 and ImageNet-1k, `CLD`-based coresets typically outperform or closely match state-of-the-art methods across subset sizes, and remain within 1% of more computationally expensive baselines even when not leading. `CLD` transfers effectively across architectures (ResNet, VGG, DenseNet), enabling proxy-to-target selection with $< 1\%$ degradation. Moreover, `CLD` is stable when using only early checkpoints, incurring negligible accuracy loss. Finally, `CLD` exhibits inherent bias reduction via per-class validation alignment, obviating the need for additional stratified sampling. Together, these properties make `CLD` a principled, efficient, stable, and transferable tool for scalable dataset optimization.

1 Introduction

Deep learning models rely on large and diverse datasets to achieve state-of-the-art performance across a wide range of tasks. However, training on such datasets is increasingly constrained by compute and memory budgets, especially in real-time or resource-limited settings. This raises a fundamental question: *Which subsets of data most effectively support generalization?* A natural answer is offered by *coresets*, compact, representative subsets of training data that retain full-dataset performance when used for training.

Coresets support a range of applications including active learning (Coleman et al., 2020), neural architecture search (Na et al., 2021; Shim et al., 2021), dataset distillation (Cazenavette et al., 2022), and continual learning (Aljundi et al., 2019; Borsos et al., 2020). However, most existing approaches are either based on heuristic criteria unrelated to generalization (Toneva et al., 2018; Belouadah et al., 2020; Rebuffi et al., 2017), or expensive second-order or bilevel optimization (Killamsetty et al., 2021a; Pruthi et al., 2020; Garg & Roy, 2023; Killamsetty et al., 2021b; Xia et al., 2024; Borsos et al., 2020), limiting scalability.

We propose a simple, scalable, and theoretically grounded alternative to coreset generation using a metric we define as the **Correlation of Loss Differences** (`CLD`). This metric quantifies how closely the loss trajectory of a training sample aligns with the average validation loss trajectory during training (Figure 1, left). Since the validation set reflects the test distribution, high positive `CLD` samples are likely to contribute positively to generalization. Selecting such samples yields compact coresets that preserve, or even improve, test accuracy by filtering out ambiguous or harmful examples (Figure 1, right).

Beyond simplicity, `CLD` provides strong theoretical guarantees. We prove that training on high-`CLD` samples achieves convergence in population risk with an error bound that closely matches full-data training, where the

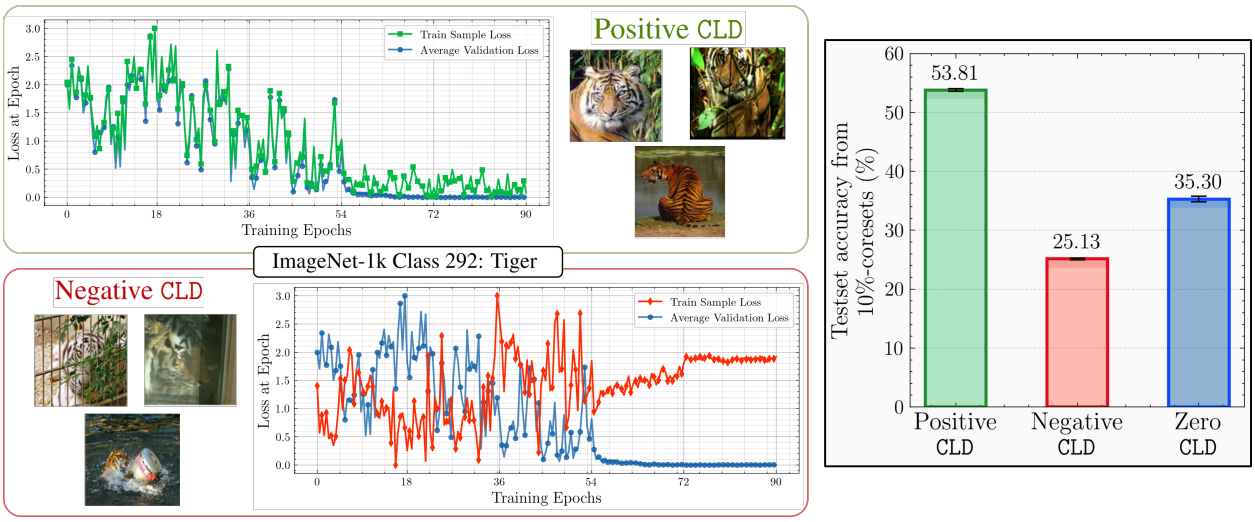

Figure 1: **Correlation of Loss Differences (CLD) at a glance. Left:** *ImageNet-1k* "Tiger" samples illustrating varying CLD scores. High-CLD samples (top row) closely track the validation loss trajectory, indicating informative and representative data. Low/negative-CLD samples (bottom row) significantly deviate, typically corresponding to atypical, ambiguous, or mislabeled examples. **Right:** Performance comparison of coresets formed by selecting equal-sized subsets of the highest 10% positive, lowest 10% negative, and 10% zero-valued CLD samples of ImageNet-1k on ResNet-18. Coresets with high-positive CLD samples achieve superior accuracy over various seeds.

excess error is explicitly governed by the sample alignment parameter κ and the validation representativeness δ (see Theorem 1). Our theory reveals that high CLD is not just sufficient but also necessary to minimize the convergence error-bound under coreset training.

We validate these findings across CIFAR-100 and ImageNet-1k, where CLD-selected coresets typically outperform or closely match state-of-the-art methods across a wide range of coreset sizes, and remain within 1% of more computationally expensive baselines even when not leading. Unlike these methods, CLD avoids costly gradients, pairwise similarities, or second-order statistics. It requires only per-sample loss values computed at training checkpoints, yielding significant gains in both computational and storage efficiency.

An additional strength of CLD is its robustness; the metric remains stable when computed using sparsely sampled training checkpoints and is consistent across random seeds, making it practical for large-scale or budgeted deployments. Furthermore, CLD coresets transfer effectively across architectures. Coresets computed using small proxy models (e.g., ResNet-18) generalize to larger models (e.g., ResNet-50, DenseNet) with performance drops consistently under 1%.

Summary of contributions:

1. **Correlation of Loss Differences for Coreset Selection.** We introduce CLD, a simple and scalable metric for coreset construction based on the correlation between a training sample's loss differences and the average validation loss trajectory, serving as a proxy for generalization, in Section 4.

2. **Theoretical Guarantees.** We develop a general convergence framework showing that training on high-CLD samples yields population risk close to full-data training, with the suboptimality explicitly governed by sample alignment and validation representativeness, in Section 5.

3. **Experimental Validation.** We show that on CIFAR-100 and ImageNet-1k, CLD-selected coresets typically outperform or closely match state-of-the-art methods across a wide range of subset sizes, and remain within 1% of more expensive baselines when not leading, in Section 6.

4. **Efficiency, Transferability, and Stability.** CLD avoids gradient and curvature computations, incurs minimal compute and storage cost, transfers across architectures via proxy models, and

remains stable under checkpoint subsampling and random seeds, making it highly practical for large-scale settings. We discuss these in Section 7 and Section 8.

2 Related Literature

The need for scalable coreset methods has led to a variety of approaches, which can be broadly grouped into *score-based*, *optimization-based*, and *training property-based* methods.

Score-based methods select training samples according to predefined metrics, often in the feature space or based on model prediction confidence. Some methods score a sample by its distance to a class center (Rebuffi et al., 2017; Castro et al., 2018; Belouadah et al., 2020), to the class feature median (e.g., `Moderate` (Xia et al., 2022)), or to other samples (Sener & Savarese, 2018). `Cal` (Margatina et al., 2021) identifies contrastive examples via the KL divergence between predictive distributions, while `Herding` (Chen et al., 2010) selects representative samples using a kernel-based approach in Hilbert space. Other methods rely on prediction probabilities from a (possibly proxy) model. For example, `Forgetting` (Toneva et al., 2018) counts how often a sample is misclassified after previously being correct, `GraNd` and `EL2N` (Paul et al., 2021) rank examples by their early-training loss gradient norm or l_2 error norm, respectively, and `AUM` (Pleiss et al., 2020) scores the *area under the margin* across training to flag potential label issues. While these approaches are simple and avoid expensive gradient or Hessian computation, they often inherit biases from their heuristic scoring rules and offer no convergence guarantees. To mitigate bias, methods such as `CCS` (Zheng et al., 2022) employ stratified sampling for diversity, while $\mathbb{D}^2$-`Pruning` (Maharana et al., 2024) combines difficulty (prediction variance) and diversity (feature density) in a graph-based framework. Nonetheless, such strategies often make restrictive assumptions to avoid noisy samples (e.g., `CCS` discards up to 30% of data) and still lack theoretical generalization guarantees.

Optimization-based methods formulate coreset selection as an explicit optimization problem, often with provable convergence guarantees. `CRAIG` (Mirzasoleiman et al., 2020) and `GradMatch` (Killamsetty et al., 2021a) select samples that align with the full-data gradient direction, while `Glister` (Killamsetty et al., 2021b) maximizes held-out validation log-likelihood. Bilevel optimization (Borsos et al., 2020) has been used to leverage influence functions (Koh & Liang, 2017) for selecting samples with maximal generalization benefit, and `GraphCut` (Iyer et al., 2021) uses submodular information measures as the objective. Recently, `BoundarySet-CCS` (Yang et al., 2024) minimized decision boundary reconstruction error while ensuring class diversity. While theoretically grounded, these approaches often require repeated optimization loops, making them computationally expensive for large datasets.

Training property-based methods exploit the dynamics of training to assess sample importance. `SloCurv` (Garg & Roy, 2023) uses second-order loss curvature statistics to identify samples with better generalization potential, and `TracIn` (Pruthi et al., 2020) tracks gradient alignment with a validation set. `TDDS` (Zhang et al., 2024) extends this idea by projecting each sample's gradient onto the accumulated gradient to quantify its true contribution, and by monitoring this projection across multiple iterations to account for fluctuations in importance over time. Although effective, such methods depend on costly first- or second-order statistics, limiting scalability.

Scalable training property-based methods reduce this overhead by measuring per-sample dynamics using only forward-pass signals. `Dyn-Unc` (He et al., 2024) summarizes the variability of the true-class probability over sliding windows and prunes by thresholding aggregated uncertainty after training. `DUAL` (Cho et al., 2025) combines this uncertainty score with a difficulty term and uses a pruning-ratio–adaptive *Beta sampling* schedule to reweight selection at high pruning ratios. In contrast, our method `CLD` ranks examples by how well their *loss-difference trajectories* align with the *class-wise validation loss trajectory*, providing an explicit generalization-alignment criterion. All three approaches admit identical minimal logging, one scalar per example per checkpoint (probability for `Dyn-Unc`/`DUAL`; loss for `CLD`), so compute and storage are directly comparable. Unlike uncertainty-only methods, however, `CLD`'s alignment objective supports a convergence guarantee (Section 5), and it avoids ratio-specific sampling schedules and their hyperparameters; we report robustness at extreme cases (e.g., coresets of size 5%) under identical logging (Section 6). *In short,* `CLD` *combines the practicality of score-based metrics (low compute/storage via scalar logging) with a validation-aligned training-dynamics signal that admits a convergence guarantee.*

3 Preliminaries and Problem Setup

We consider the supervised learning problem of learning a mapping from the input space to the output space, $\mathbf{X} \to \mathbf{Y}$, where $\mathbf{X} \subseteq \mathbb{R}^d$ and $\mathbf{Y} \subseteq \mathbb{R}$. The training dataset $\mathbf{S}$ consists of N samples drawn from an unknown distribution $\mathbf{D} = \mathbf{X} \times \mathbf{Y}$, with each sample denoted as $\vec{z}_i = (\vec{x}_i, y_i)$. Thus, $\mathbf{S} = \{\vec{z}_1, \ldots, \vec{z}_N\}$. Additionally, we assume access to a query (held-out validation) set $\mathbf{V} \sim \mathbf{D}^Q = \{\vec{q}_1, \ldots, \vec{q}_Q\}$ containing Q samples, which represents the true distribution $\mathbf{D}$.

A learning algorithm $\mathbf{A}$ (e.g., SGD) is used to train a model with parameters $\theta \in \mathbb{R}^p$ on the training set $\mathbf{S}$ over T iterations. We denote the model parameters at iteration t of training on $\mathbf{S}$ as $\theta^t_{\mathbf{S}}$, where $\theta^0_{\mathbf{S}}$ corresponds to the random initialization prior to the first update. The performance of the model at step t on a sample $\vec{z}_m$ is evaluated using a loss function $\ell(\theta^t_{\mathbf{S}}, \vec{z}_m) : \mathbb{R}^p \times \mathbb{R}^d \to \mathbb{R}$, which quantifies the prediction error on $\vec{z}_m$ at that point in training.

The goal of training is to minimize the *population risk* $R_{\mathbf{D}}(\theta)$,

$$\arg\min_{\theta} R_{\mathbf{D}}(\theta) = \arg\min_{\theta} \mathop{\mathbb{E}}_{\vec{z}\sim\mathbf{D}}[\ell(\theta, \vec{z})]. \tag{1}$$

However, since $\mathbf{D}$ is unknown, we instead minimize the *empirical risk* $\hat{R}(\theta, \mathbf{S})$,

$$\arg\min_{\theta} \hat{R}(\theta, \mathcal{S}) = \arg\min_{\theta} \left(\frac{1}{N} \sum_{m=1}^{N} \ell(\theta, \vec{z}_m) \right). \tag{2}$$

The gradient of the loss with respect to the parameters θ at step t for a sample $\vec{z}_i$ is denoted as $\nabla_\theta \ell(\theta^t_{\mathbf{S}}, \vec{z}_i)$. The average gradient over the validation set ($G_{\mathbf{V}}$) is,

$$G_{\mathbf{V}}(\theta^t_{\mathbf{S}}) = \frac{1}{Q} \sum_{j=1}^{Q} \nabla_\theta \ell(\theta^t_{\mathbf{S}}, \vec{q}_j) \tag{3}$$

4 Correlation of Loss Differences (CLD)

We now define the core quantity used in our method, the correlation of per-sample loss trajectories with the validation set.

Loss Trajectories For every sample $\vec{z}$ we record the per-iteration change in loss during the model training run, and collect these T increments in a *loss-difference trajectory*

$$\vec{\Delta}(\vec{z}) \;=\; \left(\ell(\theta^1_{\mathbf{S}}, \vec{z}) - \ell(\theta^0_{\mathbf{S}}, \vec{z}),\; \ldots,\; \ell(\theta^T_{\mathbf{S}}, \vec{z}) - \ell(\theta^{T-1}_{\mathbf{S}}, \vec{z})\right) \in \mathbb{R}^T. \tag{4}$$

The *validation-average trajectory* is defined similarly as,

$$\vec{\Delta}'_{\mathbf{V}} \;=\; \left(\frac{1}{Q} \sum_{j=1}^{Q} \left[\ell\left(\theta^1_{\mathbf{S}}, \vec{q}_j\right) - \ell\left(\theta^0_{\mathbf{S}}, \vec{q}_j\right)\right],\; \ldots,\; \frac{1}{Q} \sum_{j=1}^{Q} \left[\ell\left(\theta^T_{\mathbf{S}}, \vec{q}_j\right) - \ell\left(\theta^{T-1}_{\mathbf{S}}, \vec{q}_j\right)\right] \right) \in \mathbb{R}^T. \tag{5}$$

Definition 1 (Correlation of Loss Differences (`CLD`))**.** *The* `CLD` *score of a training sample $\vec{z}_m \in \mathbf{S}$ is the correlation between the sample's loss trajectory $\vec{\Delta}_m$ and the average loss trajectory of the validation set $\mathbf{V}$:*

$$\texttt{CLD}(\vec{z}_m) \coloneqq \rho\left(\vec{\Delta}_m, \vec{\Delta}'_{\mathbf{V}}\right), \tag{6}$$

where ρ is the correlation metric. In our experiments, we employ Pearson correlation (Pearson, 1895) due to its scale invariance and computational simplicity. Intuitively, the `CLD` metric quantifies how well a training sample's loss dynamics align with the aggregate loss trajectory of the validation set, which serves as a proxy

for generalization behavior. Samples with higher CLD values are deemed more influential and can thus be prioritized for coreset construction. We investigate this hypothesis both theoretically and empirically in the following sections.

While Definition 1 defines CLD using a global validation trajectory, our practical implementation uses class-specific averages to ensure semantic alignment; see Section 4.1.

4.1 Coreset Selection Procedure

We first train a source model $\theta_{\mathbf{S}}$ on the full dataset $\mathbf{S}$, recording per-epoch losses for all training and validation samples. We then compute $\vec{\Delta}_m$ and the *class-specific average validation trajectory* $\vec{\Delta}'_{\mathbf{V},c}$ for each class c.

$$\vec{\Delta}'_{\mathbf{V},c} \coloneqq \left(\frac{1}{|\mathbf{V}_c|} \sum_{\vec{q}_j \in \mathbf{V}_c} \left[\ell(\theta^1_{\mathbf{S}}, \vec{q}_j) - \ell(\theta^0_{\mathbf{S}}, \vec{q}_j) \right], \ldots, \frac{1}{|\mathbf{V}_c|} \sum_{\vec{q}_j \in \mathbf{V}_c} \left[\ell(\theta^T_{\mathbf{S}}, \vec{q}_j) - \ell(\theta^{T-1}_{\mathbf{S}}, \vec{q}_j) \right] \right) \in \mathbb{R}^T, \tag{7}$$

$$\text{where} \quad \mathbf{V}_c \coloneqq \{ \vec{q}_j \in \mathbf{V} : y_{q_j} = c \}. \tag{8}$$

In accordance with standard practice for coreset selection, we score samples within each class independently. For a training sample $\vec{z}_m \in \mathbf{S}$ with label $y_m = c$, its CLD score is the Pearson correlation between its trajectory and the corresponding class-specific validation trajectory:

$$\texttt{CLD}(\vec{z}_m) \;\coloneqq\; \rho\big(\vec{\Delta}(\vec{z}_m),\, \vec{\Delta}'_{\mathbf{V},c}\big) \quad \forall \vec{z}_m : y_m = c. \tag{9}$$

After computing all scores, we select the top-k_c training samples in each class c to form a class-balanced coreset

$$\mathbf{C} \;=\; \bigcup_{c=1}^{C} \mathbf{C}_c, \qquad \mathbf{C}_c \;=\; \text{Top-}k_c\big(\{\vec{z}_m \in \mathbf{S} : y_m = c\},\, \texttt{CLD}\big), \tag{10}$$

with total size fixed in advance as $k = \sum_{c=1}^{C} k_c$. This per-class selection strategy ensures both label balance and stability of dynamics within semantic categories, improving the robustness and interpretability of the resulting coreset.

A key advantage is architectural flexibility. CLD scores can be computed using a proxy model and transferred to larger or deeper architectures. The full coreset selection procedure is summarized in Appendix A.

5 Theoretical Analysis of CLD-Coresets

We now provide a theoretical justification for selecting high-CLD samples, showing that such coresets yield convergence guarantees close to full-data training under the following assumptions.

Assumption 1 (L-smoothness)**.** *For every fixed sample $\vec{z}$, define $f(\theta) \coloneqq \ell(\theta, \vec{z})$. Then f is L-smooth in θ, i.e.,*

$$f(y) \;\le\; f(x) \;+\; \langle \nabla f(x),\, y - x \rangle \;+\; \frac{L}{2}\, \|y - x\|_2^2, \qquad \forall x, y \in \mathbb{R}^p. \tag{11}$$

Consequently, both the population risk $R_{\mathbf{D}}(\cdot)$ and the empirical risk $\hat{R}(\cdot)$ are also L-smooth.

Assumption 2 (Bounded Gradient Norm)**.** *There exists $B > 0$ such that, for all θ and every training sample $\vec{z}_m \in \mathbf{S}$ and validation sample $\vec{q}_j \in \mathbf{V}$, $\|\nabla_\theta \ell(\theta, \vec{z}_m)\|_2 \le B$, and $\|\nabla_\theta \ell(\theta, \vec{q}_j)\|_2 \le B$. Consequently, for any index set $\mathcal{C} \subseteq \{1, \ldots, N\}$,*

$$\left\| \frac{1}{|\mathcal{C}|} \sum_{m \in \mathcal{C}} \nabla_\theta \ell(\theta, \vec{z}_m) \right\|_2 \le B, \qquad \|G_{\mathbf{V}}(\theta)\|_2 \le B, \tag{12}$$

where $G_{\mathbf{V}}(\theta) \coloneqq \dfrac{1}{Q} \displaystyle\sum_{j=1}^{Q} \nabla_\theta \ell(\theta, \vec{q}_j)$ is the validation-average gradient.

Assumption 3 (Validation Representativeness)**.** *With probability at least $1-\delta'$, the validation gradient $G_{\mathbf{V}}(\cdot)$ at every iterate θ encountered during training satisfies*

$$\|G_{\mathbf{V}}(\theta) - \nabla_\theta R_{\mathbf{D}}(\theta)\|_2 \leq \delta, \quad \textit{where} \quad \delta = \mathcal{O}(B/\sqrt{Q}). \tag{13}$$

These assumptions mirror those commonly adopted in analyses of training dynamics (Pruthi et al., 2020; Ilyas et al., 2022; Veen et al., 2020; Clemmensen & Kjærsgaard, 2022; Zhang et al., 2022); we merely state Assumption 3 explicitly for transparency, even though it is typically invoked implicitly and is widely regarded as reasonable.

Remark 1 (Per-Class Validation Trajectories)**.** *In our implementation, we compute* `CLD` *using class-specific validation trajectories $\vec{\Delta}'_{\mathbf{V},c}$ rather than a single global trajectory. This refinement aligns with standard coreset practices that enforce class balance, which reduces the variance of the correlation estimates by matching each training sample with the validation subset most relevant to its semantic label. The theoretical guarantees stated here continue to hold, as long as the per-class validation subsets satisfy the representativeness condition in Assumption 3 when interpreted class-conditionally.*

Theorem 1 (Convergence with `CLD`-Coresets)**.** *Consider a gradient descent algorithm trained over T iterations on a training dataset $\mathbf{S}$ with a held-out validation set $\mathbf{V}$. Given Assumptions 1 to 3, let the learning rate satisfy $0 < \eta \leq 1/L$. Let $\theta^t_{\mathbf{C}}$ denote the parameters at iteration t when training on a coreset $\mathbf{C}$.*

Then, training on the coreset $\mathbf{C}$, consisting of samples with high `CLD` *scores:*

$$\mathbf{C} \;=\; \left\{\, \vec{z}_m \in \mathbf{S} \;:\; \texttt{CLD}(\vec{z}_m) \geq 1-\epsilon \,\right\}, \qquad \epsilon > 0, \;\; \epsilon \to 0, \tag{14}$$

guarantees that

$$\min_{0\leq t<T} \left\|\nabla_\theta R_{\mathbf{D}}(\theta^t_{\mathbf{C}})\right\|_2^2 \;\leq\; \frac{2\left[R_{\mathbf{D}}(\theta^0_{\mathbf{C}}) - R_{\inf}\right]}{\eta T} + L\eta B^2 + \left(B\sqrt{2\kappa} + \delta\right)^2, \tag{15}$$

where $R_{\inf} := \inf_\theta R_{\mathbf{D}}(\theta)$, and $\kappa \geq 0$ is an alignment-gap *term that quantifies the mismatch between the average coreset gradient and the validation proxy gradient $G_{\mathbf{V}}(\theta)$ along training (see Appendix B for the formal definition). Intuitively, κ decreases as the selected samples'* `CLD` *scores increase and as the coreset grows, and $\kappa \to 0$ as $\epsilon \to 0$.*

Proof Sketch. The proof is based on the observation that the change in population risk across training steps can be approximated by the inner product between the gradient of the risk and the update direction. A high `CLD` score implies a strong correlation between a sample's loss-change trajectory and that of the validation set, which in turn suggests consistent alignment between the sample's gradient and the validation gradient.

Due to the L-smoothness of the loss function, this alignment persists even when training on the coreset, allowing us to bound the cosine similarity between the average coreset gradient and the true risk gradient. This leads to a controlled approximation error in the optimization update. The total error term $(B\sqrt{2\kappa}+\delta)^2$ is governed by three factors: the `CLD` scores of selected samples, the deviation between the coreset and full-data parameter trajectories, and the quality of the validation set as a proxy for the true distribution. Full details and supporting lemmas are provided in Appendix B. □

Interpreting the Theory Under the stated assumptions, training on the full dataset $\mathbf{S}$ yields the convergence bound

$$\min_{0\leq t<T} \left\|\nabla_\theta R_{\mathbf{D}}(\theta^t_{\mathbf{S}})\right\|_2^2 \leq \frac{2\left[R_{\mathbf{D}}(\theta^0_{\mathbf{S}}) - R_{\inf}\right]}{\eta T} + L\eta B^2. \tag{16}$$

Theorem 1 shows that training on a high-`CLD` coreset achieves a similar bound, up to an additive deviation term $(B\sqrt{2\kappa}+\delta)^2$. This deviation captures the alignment of the coreset with the validation dynamics (κ), and the representativeness of the validation set (δ).

The alignment term κ reflects both the informativeness of selected samples and the size of the coreset. Higher `CLD` scores indicate stronger agreement with validation loss trajectories and thus tighter gradient

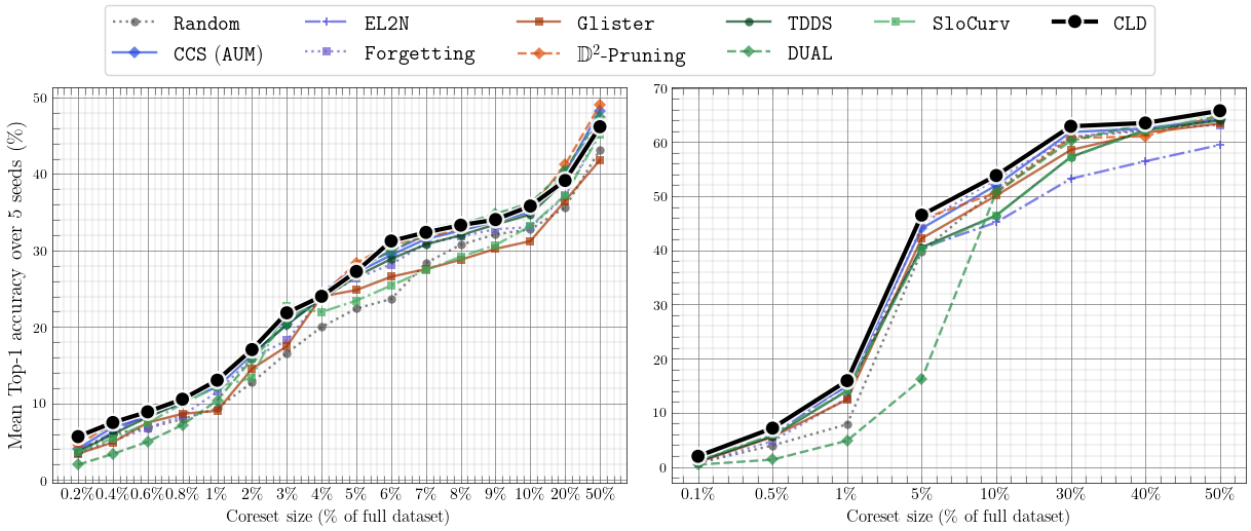

(a) CIFAR-100 (b) ImageNet-1k

Figure 2: Test accuracy (mean over five seeds) for representative coreset selection methods on CIFAR-100 and ImageNet-1k with ResNet-18. `CLD` consistently matches or outperforms baselines across dataset sizes. *(X-axis uses a non-uniform coreset-size grid.)* Color map: blues (score-based), oranges (optimization-based), greens (training-property-based), black (`CLD`). Complete numerical results are available in Appendix C.

alignment, reducing κ. Additionally, larger coresets more faithfully approximate full-data training dynamics, also lowering κ. When the coreset size is fixed, the theorem implies that selecting higher-`CLD` samples improves convergence by minimizing this deviation. Thus, `CLD`-based selection emerges as a principled and necessary criterion for preserving the optimization behavior of full-data training.

Corollary 1 (Necessity of High `CLD` for Good Coresets)**.** *Under the hypotheses of Theorem 1, achieving convergence rates comparable to full-data training* necessarily *requires that the selected samples exhibit near-maximal* `CLD` *scores and that the validation set provides a reliable proxy for the true risk gradient. Fulfilling these necessary conditions ensures the optimization dynamics induced by the coreset remain well-aligned with those of full-data training.*

6 Experimental Evaluation

We evaluate `CLD` empirically, focusing on its effectiveness and transferability.

Experimental Setup We benchmark on CIFAR-100 (Krizhevsky et al., 2009) and ImageNet-1k (Russakovsky et al., 2015). CIFAR-100 has 50,000 training and 10,000 test images across 100 classes; ImageNet-1k has $\sim$1.28M training images and a 50,000-image validation set across 1,000 classes. For each random seed, we form a *classwise* held-out validation split from the training data (10% for CIFAR-100; 1% for ImageNet-1k), ensuring equal per-class representation; a different split is generated per seed, and the resulting train/validation partitions are reused across all baselines for fairness. Unless otherwise specified, ResNet-18 (He et al., 2016) is the default architecture for `CLD` scoring and for training on selected coresets. Coresets are constructed *per seed* in a class-balanced manner by selecting, within each class, the top-ranked samples under `CLD`. Subset sizes range from 0.2%–100% on CIFAR-100 and 0.1%–100% on ImageNet-1k. We report the mean and standard deviation over 5 independent seeds.

Baselines. We compare against representative state-of-the-art methods from three families: *score-based* (`Forgetting` (Toneva et al., 2018), `EL2N` (Paul et al., 2021), and `CCS` (Zheng et al., 2022) using `AUM` (Pleiss et al., 2020)), *optimization-based* (`Glister` (Killamsetty et al., 2021b), $\mathbb{D}^2$-`Pruning` (Maharana et al., 2024)), and *training-property–based* (`TDDS` (Zhang et al., 2024), `SloCurv` (Garg & Roy, 2023), `DUAL` (Cho et al., 2025)), plus `Random`. We use implementations from the DeepCore (Guo et al., 2022) library when available, and otherwise rely on official GitHub repositories. All methods are run under a consistent training setup (40

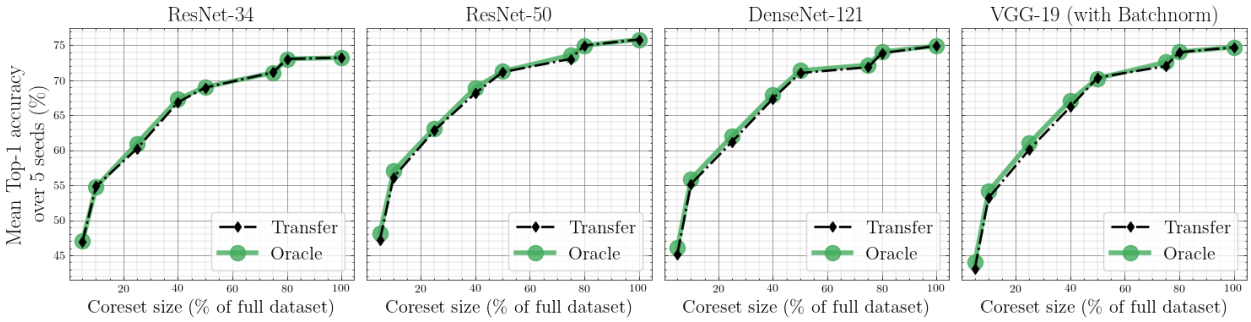

Figure 3: *Transferability of* CLD*-based coresets across architectures on ImageNet-1k.* Each subplot reports test accuracy (mean over five runs) for target models trained on coresets of varying sizes. **Transfer** coresets (dashed black, diamonds) are selected using ResNet-18; **Oracle** coresets (solid green, circles) are computed by the target itself. Transferred coresets are within 1% of oracle coresets across all targets and sizes.

pretraining epochs where required), without any additional fine-tuning or regularization. To ensure fairness, all baselines, including ours, select and train coresets using the same backbone (ResNet-18).

Transferability protocol. On ImageNet-1k we additionally test cross-architecture transfer. We compute **Transfer** coresets using ResNet-18 and apply them to ResNet-34, ResNet-50, VGG-19, and DenseNet-121. We compare this to an **Oracle** setting where each target model computes its own CLD scores and coresets from its dynamics.

Results and Observations Figure 2 summarizes performance on CIFAR-100 and ImageNet-1k compared to other methods. Across both datasets, CLD consistently matches or outperforms the strongest baselines from each family. The most competitive alternatives are $\mathbb{D}^2$-Pruning and DUAL, though both degrade at very small coreset sizes. On CIFAR-100, Glister, DUAL, CCS (AUM) can slightly edge out CLD at larger subsets (by $<1\%$), whereas CLD consistently leads on ImageNet-1k. At large subset sizes, CLD converges to full-data performance with negligible deviation from the strongest baseline. Full numerical tables (and additional methods beyond those plotted) are deferred to Appendix C to avoid clutter. A complementary analysis of the subset fraction required to match full-data accuracy is presented in Appendix D.2.

For cross-architecture transfer on ImageNet-1k, Figure 3 shows that **Transfer** coresets selected with ResNet-18 closely track **Oracle** coresets computed by the target model itself. The gap remains below 1% across ResNet-34, ResNet-50, VGG-19, and DenseNet-121 and across coreset sizes, including transfers across architecture families (ResNet $\rightarrow$ DenseNet/VGG).

Takeaways CLD achieves near-optimal accuracy across subset sizes while incurring the lowest compute and storage overhead among strong baselines, and its coresets transfer effectively from lightweight proxies to larger targets. Together, these properties make CLD a scalable, reliable choice for coreset selection in both single-architecture and cross-architecture regimes.

7 Computational and Storage Efficiency

Beyond accuracy, a practical coreset method should keep both *compute* and *storage* costs low. CLD does so by relying only on per-sample *loss scalars* that standard training already produces; no per-sample gradients, Hessians, or pairwise similarities are required. The only extra work is a forward-only sweep over a small held-out query set each proxy epoch ($Q \ll N$) to record query losses. In contrast, gradient/adversarial methods incur extra backward passes, while similarity/nearest-neighbor methods require feature extraction and large feature caches. We quantify the *end-to-end* compute cost (selection *plus* training on the selected coreset) and the storage overhead in detail in Appendix E and summarize the symbolic complexity below.

Notation and setup. We measure compute in floating-point operations (FLOPs) and report storage overheads:

Table 1: End-to-end compute and *storage overhead* for `CLD` and baselines. Storage column lists *method-specific extras during selection only.* Notation in Section 7.

Method	Computational cost (selection + coreset training)	Storage overhead (method-specific extras)
`Herding`	$3NT_{\text{proxy}}f \;+\; Nf \;+\; \mathcal{O}(Ndk) \;+\; 3kTf_{\text{large}}$	$\mathcal{O}(Nd)$ [features] (+ optional $\mathcal{O}(k^2)$ Gram)
`Forgetting`	$3NT_{\text{early}}f_{\text{large}} \;+\; 3kT_{\text{late}}f_{\text{large}}$	$\mathcal{O}(N)$ [per-sample counter]
`AUM`	$3NT_{\text{proxy}}f \;+\; 3kTf_{\text{large}}$	$\mathcal{O}(N)$ [running sums]
`Cal`	$3kT_{\text{proxy}}f \;+\; Uf \;+\; \mathcal{O}(U\kappa d) \;+\; 3kTf_{\text{large}}$	$\mathcal{O}(Ud)$ [proxy features]
`GraNd`	$3NT_{\text{early}}Rf_{\text{large}} \;+\; 3NT_{\text{early}}Rf_{\text{large}} \;+\; 3kT_{\text{late}}f_{\text{large}}$	$\mathcal{O}(N)$ [scores/logs]
`EL2N`	$3NT_{\text{early}}Rf_{\text{large}} \;+\; 3kT_{\text{late}}f_{\text{large}}$	$\mathcal{O}(N)$ [scores]
`Moderate`	$3NT_{\text{proxy}}f \;+\; Nf \;+\; \mathcal{O}(Nd + N\log N) \;+\; 3kTf_{\text{large}}$	$\mathcal{O}(Nd)$ [proxy features]
$\mathbb{D}^2$`-Pruning`	$3NT_{\text{proxy}}f \;+\; Nf \;+\; \mathcal{O}(N\kappa d) \;+\; \mathcal{O}(HN\kappa) \;+\; 3kTf_{\text{large}}$	$\mathcal{O}(Nd) + \mathcal{O}(N\kappa)$ [features + kNN graph]
`CRAIG`	$3NT_{\text{proxy}}f \;+\; \mathcal{O}\big(A\,(Nk + N\log(1/\epsilon))\,D_{\text{eff}}\big) \;+\; 3kTf_{\text{large}}$	$\mathcal{O}\big(N(F{+}c)\big)$ [per-anchor embeddings]
`Glister`	$3kTf_{\text{large}} \;+\; \mathcal{O}\big((kQ + N\log(1/\epsilon))\,f_{\text{large}}\,T/\gamma\big)$	$\mathcal{O}(Q)$ [validation cache]
`GraphCut`	$3NT_{\text{proxy}}f \;+\; Nf \;+\; \mathcal{O}(N^2k) \;+\; 3kTf_{\text{large}}$	$\mathcal{O}(N^2)$ [pairwise similarities]
`SloCurv`	$3NT_{\text{proxy}}f \;+\; 3N(R{+}1)f \;+\; 3kTf_{\text{large}}$	$\mathcal{O}(N) + \mathcal{O}(Rd)$ [running stats + probe dirs]
`TDDS`	$3NT_{\text{proxy}}f \;+\; 3NT_{\text{proxy}}f \;+\; 3kTf_{\text{large}}$	$\mathcal{O}(NJ)$ [windowed logs]
`Dyn-Unc`	$3NT_{\text{proxy}}f \;+\; 3kTf_{\text{large}}$	$\mathcal{O}(NJ)$ [windowed logs]
`DUAL`	$3NT_{\text{proxy,early}}f \;+\; 3kTf_{\text{large}}$	$\mathcal{O}(NJ)$ [windowed logs]
CLD (Ours)	$\mathbf{3NT_{\text{proxy}}f \;+\; QT_{\text{proxy}}f \;+\; 3kTf_{\text{large}}}$	$\mathcal{O}\big((\mathbf{N}{+}\mathbf{Q})\mathbf{T}_{\text{proxy}}\big)$ [loss logs]

- **Data and epochs.** N training samples, Q query samples; T epochs for the *large* model, T_{proxy} for the *proxy*; T_{early} (early scoring), $T_{\text{proxy,early}}$ (early proxy epochs in `DUAL`).
- **Model cost convention.** Large model forward cost f_{large}, proxy forward cost f with $f \ll f_{\text{large}}$. One backward ≈ 2 forwards $\Rightarrow$ one training step ≈ 3 forwards per example.
- **Subset/problem.** k coreset size; d input dimension; c classes; R repeats (restarts/probes); γ reselection interval.
- **CRAIG embeddings.** F penultimate-feature dimension; $D_{\text{eff}} := F{+}c$ is the embedding size used by `CRAIG`.
- **Method-specific.** J window length (`Dyn-Unc`/`DUAL`/`TDDS`); H message-passing rounds ($\mathbb{D}^2$`-Pruning`); κ kNN degree; U unlabeled-pool size (`Cal`); γ_{anc} anchor spacing and $A{=}T_{\text{proxy}}/\gamma_{\text{anc}}$ anchors (`CRAIG`); ϵ stochastic-greedy tolerance; λ trade-off in `GraphCut`.

Results and observations (compute). As summarized in Table 1, methods that score *during early training of the large model* (e.g., `Forgetting`, `EL2N`, `GraNd`) require one or more full sweeps over all N examples with the large network for T_{early} epochs (and sometimes R repeats), so their selection cost includes terms like $3NT_{\text{early}}R\,f_{\text{large}}$, making them compute-inefficient even if the coreset used later is small. Optimization-with-reselection methods (e.g., `Glister`) add frequent subset updates every γ epochs, driving $\mathcal{O}\big((kQ + N\log(1/\epsilon))\,f_{\text{large}}\,T/\gamma\big)$ on top of $3kT\,f_{\text{large}}$. Feature/graph–based selectors (`Herding`, `Moderate`, $\mathbb{D}^2$`-Pruning`, `Cal`) pay $3NT_{\text{proxy}}f$ plus at least one Nf encoding pass (sometimes graph/kNN work). By

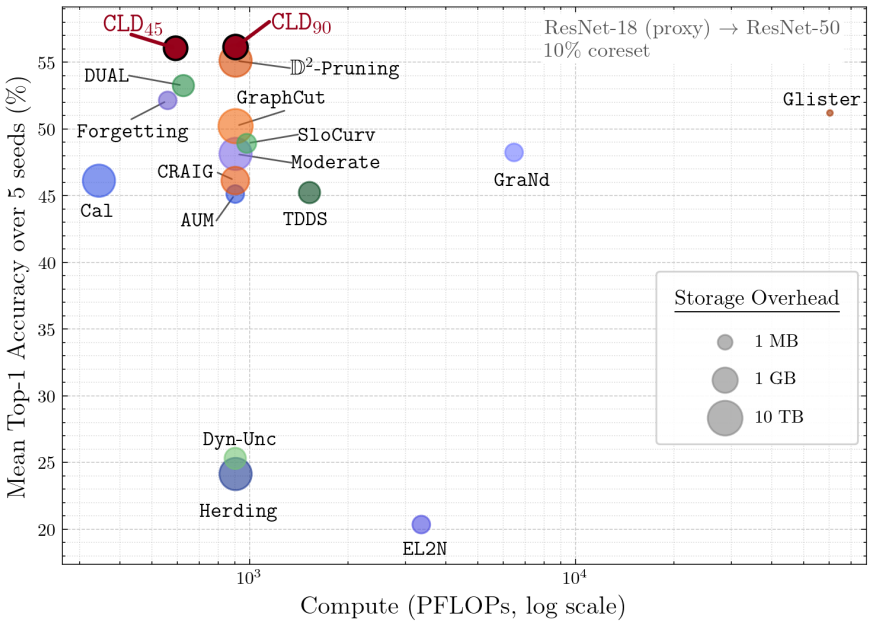

Figure 4: Efficiency summary: Accuracy vs. Compute (x-axis, log scale); bubble size is proportional to the selection-stage storage overhead. The plot uses an illustrative setup for concreteness: selecting 10% coresets of ImageNet-1k with a ResNet-18 proxy and training a ResNet-50 on the coreset (see Appendix E). Both $\texttt{CLD}_{90}$ (all proxy epochs) and $\texttt{CLD}_{45}$ (first 45 proxy epochs) are shown; the latter achieves similar accuracy at roughly half the selection compute. A similar trend is observed for `DUAL` when restricted to early proxy epochs (which we discuss in Section 8), highlighting that early-epoch scoring can improve efficiency without harming performance.

contrast, `CLD` uses only proxy training and cheap per-epoch query forwards:

$$\text{Compute}_{\texttt{CLD}} \;=\; 3NT_{\text{proxy}}f \;+\; QT_{\text{proxy}}f \;+\; 3kT\, f_{\text{large}},$$

with no gradient/Hessian sweeps, no adversarial steps, and no pairwise similarities.

Results and observations (storage). To make storage comparisons transparent, Table 1 reports *selection-stage storage overhead only*, i.e., method-specific extras beyond storing the large model's weights. Early-training methods (`Forgetting`, `EL2N`, `GraNd`, `AUM`) need only $\mathcal{O}(N)$ scalars; windowed-uncertainty methods (`Dyn-Unc`, `DUAL`, `TDDS`) add $\mathcal{O}(NJ)$ logs. `CRAIG` stores $\mathcal{O}\big(N(F{+}c)\big)$ embeddings, similarity/feature methods cache $\mathcal{O}(Nd)$ (plus $\mathcal{O}(N\kappa)$ graphs), and `GraphCut` is $\mathcal{O}(N^2)$. `CLD` uses only scalar loss logs $\mathcal{O}\big((N{+}Q)T_{\text{proxy}}\big)$.

A visual summary. Figure 4 summarizes the trade-off between accuracy (y-axis) and end-to-end compute (x-axis, log scale), with bubble size proportional to the *selection-stage storage overhead*. Points in the upper-left with small bubbles are closest to the "Pareto-efficient" frontier, combining high accuracy with low compute and storage cost. To provide a concrete, quantitative context for these trade-offs, the plot is generated using an illustrative setup: selecting 10% coresets of ImageNet-1k with a ResNet-18 proxy, then training a ResNet-50 on the chosen coreset (see Appendix E for details). In this setting, methods that score *during early training of the large model* (e.g., `GraNd`, `EL2N`) and those with frequent reselection (e.g., `Glister`) appear far to the right due to large compute costs, while feature/similarity-based selectors (`Herding`, `Moderate`, `Cal`, `D²-Pruning`) have large bubbles from $\mathcal{O}(Nd)$ feature caches. `CLD` lies near the efficient frontier: its selection cost is proxy-only plus lightweight query forwards, and its storage is just scalar loss logs. We also show $\texttt{CLD}_{90}$ (scores derived using loss values from all proxy epochs) and $\texttt{CLD}_{45}$ (first 45 epochs only); the latter cuts selection compute nearly in half while preserving accuracy (discussed in Section 8). This mirrors observations for `DUAL`, which also achieves minimal accuracy drop by using only

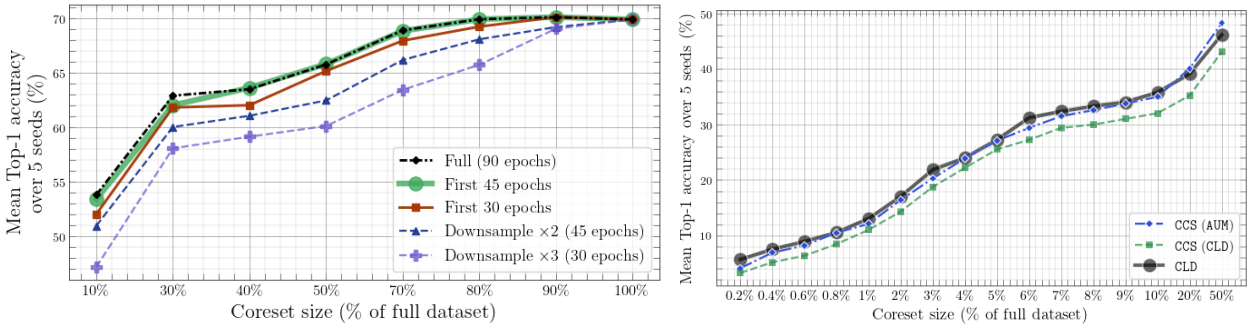

(a) Test accuracy when CLD is computed from early or subsampled checkpoints. Stability holds even at coarse resolution. *(X-axis uses a non-uniform coreset-size grid.)*

(b) *Ablation on bias reduction.* CCS-style stratified sampling on top of CLD consistently reduces accuracy across coreset sizes on CIFAR-100.

Figure 5: **Stability and bias.** (a) CLD is stable under reduced temporal resolution; (b) external stratified sampling is unnecessary, and often harmful, for CLD.

early proxy epochs, underscoring that temporal truncation can further improve efficiency without sacrificing performance. For clarity, the figure uses shades of blue for score-based methods, shades of orange for optimization-based methods, shades of green for training-property-based methods, and dark red for CLD.

8 Discussion

We discuss practical considerations and empirical findings that further illustrate the applicability of CLD.

Stability under temporal subsampling. We first assess robustness to reduced temporal resolution on ImageNet-1k with ResNet-18. CLD is computed either from the first 30 or 45 checkpoints (out of 90) or from trajectories subsampled at 2× or 3× lower frequency, while training still runs for all 90 epochs. As shown in Figure 5a, using only early checkpoints (30/45) yields accuracy nearly identical to the full-trajectory setting, indicating that the informative signal is captured early in training. 2× subsampling preserves accuracy, and even 3× subsampling incurs only a minor degradation due to reduced temporal resolution.

Bias reduction and stratified sampling. Several methods incorporate bias-reduction mechanisms, such as CCS (Zheng et al., 2022), which stratifies selection across score percentiles to promote diversity. In contrast, CLD leverages per-class validation trajectories, yielding a generalization-aware signal that naturally balances classes and downweights noisy or redundant samples. As shown in Figure 5b, applying CCS-style stratified sampling on top of CLD scores consistently *reduces* accuracy across coreset sizes on CIFAR-100. This contrasts with metrics like AUM, where CCS can be beneficial; for CLD, percentile quotas perturb its validation-aligned ranking and reintroduce less informative points.

Validation proxy: composition and size matter. Our theoretical guarantees for CLD require that the validation set be a faithful proxy for the test distribution (Assumption 3 in Section 5). To understand this, we ask: *How sensitive is* CLD *to the composition of the validation set, and does bias in this validation set affect downstream coreset quality?* To probe this, we split CIFAR-100's 50k training set into a classwise 25k/25k train/pool partition. From the pool, we constructed 5000 example validation sets using five heuristics based on publicly available memorization scores (Feldman & Zhang, 2020), denoted mem. Intuitively, low-mem points correspond to canonical, stereotypical examples (often helpful for transfer and exploited by methods such as SloCurv), while high-mem points surface atypical or mislabeled examples. These heuristics, therefore, let us bias the validation set toward "typical" or "atypical" regions of the data. We trained ResNet-18 proxies on the 25k train split, computed CLD with respect to each heuristic-based validation set, built class-balanced coresets, and fine-tuned ResNet-18 across coreset sizes (five seeds; see Figure 6b). As shown in Figure 6a, the non-random heuristics yield validation sets with markedly different mem profiles. Two clear patterns emerge. First, validation sets biased toward HIGHEST-mem examples consistently degrade performance across

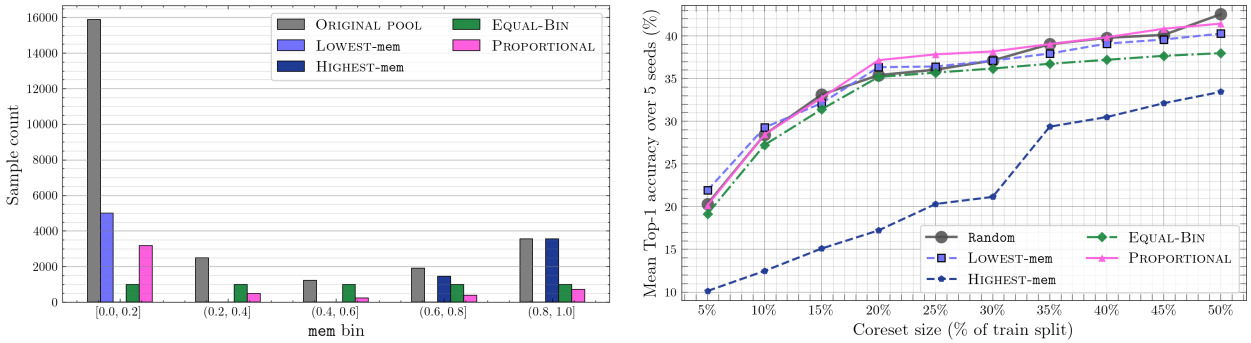

(a) **mem Scores of Validation Sets Tested.** Counts per mem bin for each heuristic (Random, Lowest-mem, Highest-mem, Equal-Bin, Proportional); the pool's original distribution is included for reference.

(b) **Effect of Validation Set Composition** CIFAR-100, ResNet-18; mean over five seeds (shaded bands: std). Validation sets are built by the five mem-based heuristics. No label cleaning was applied.

Figure 6: Validation proxy study on CIFAR-100: (a) distributional differences induced by mem-based heuristics; (b) downstream impact on CLD coreset performance.

coreset sizes: overrepresenting atypical or mislabeled samples lowers accuracy and hinders learning. Second, validation sets built from Lowest-mem examples generally support stronger generalization, but retaining *some* high-mem points is beneficial for capturing long-tail behavior likely present in the test distribution. In our runs, Proportional sampling, drawing examples according to the pool's original mem distribution, was the most reliable overall, and would likely improve further if mislabeled points were filtered or downweighted (which we did *not* do in this study). These findings underscore that CLD's effectiveness depends critically on the quality of the validation signal: coresets cannot exceed the fidelity of the validation dynamics they are aligned with. This motivates future work on principled procedures to build clean, representative validation sets (e.g., robust to label noise) and to select validation sizes that balance reliability with efficiency.

Overall, CLD already achieves implicit bias reduction via validation alignment; external stratified sampling is unnecessary and often counterproductive. We provide further results, including seed-wise stability (Appendix D.1) and connections to influence functions and training data attribution methods (Appendix F), in the appendix.

9 Limitations

While CLD is scalable and effective, it does have limitations. First, it requires access to training loss trajectories across multiple checkpoints, which may not be feasible in settings where models are deployed as black boxes or when fine-tuning from pretrained checkpoints without full retraining. Second, although CLD requires a hold-out validation set, this reduces the number of samples for training.

10 Conclusion

We introduced *Correlation of Loss Differences* (CLD), a simple, scalable metric for identifying data that aligns with generalization. By relying only on per-sample losses across training checkpoints, without gradients, pairwise similarities, or second-order information, CLD enables principled coreset selection with low compute and storage cost. Across CIFAR-100 and ImageNet-1k, CLD matches or outperforms state-of-the-art methods over a wide range of subset sizes and attains full-data accuracy with substantially smaller subsets. CLD-selected coresets also transfer across architectures (ResNet, VGG, DenseNet) with $<1\%$ degradation, remain stable when using only early checkpoints, and inherently reduce bias via per-class validation alignment, obviating additional stratified sampling. Our theory further shows that the convergence gap under coreset training is controlled by sample–validation alignment and the representativeness of the validation set. Taken together, these properties make CLD a practical tool for large-scale, budgeted training and a principled foundation for future work on robust validation design and budget-aware data selection.

References

Rahaf Aljundi, Min Lin, Baptiste Goujaud, and Yoshua Bengio. Gradient based sample selection for online continual learning. *Advances in neural information processing systems (NeurIPS)*, 32, 2019.

Juhan Bae, Wu Lin, Jonathan Lorraine, and Roger Baker Grosse. Training data attribution via approximate unrolling. In *The Thirty-eighth Annual Conference on Neural Information Processing Systems (NeurIPS)*, 2024.

S Basu, P Pope, and S Feizi. Influence functions in deep learning are fragile. In *International Conference on Learning Representations (ICLR)*, 2021.

Eden Belouadah, Adrian Popescu, and Ioannis Kanellos. Initial classifier weights replay for memoryless class incremental learning. In *BMVC 2020-The 31st British Machine Vision Virtual Conference (BMVC)*, pp. 1–13, 2020.

Zalán Borsos, Mojmir Mutny, and Andreas Krause. Coresets via bilevel optimization for continual learning and streaming. *Advances in neural information processing systems (NeurIPS)*, 33:14879–14890, 2020.

Léon Bottou. Large-scale machine learning with stochastic gradient descent. In *Proceedings of COMPSTAT'2010: 19th International Conference on Computational Statistics, Paris France, August 22-27, 2010 Keynote, Invited and Contributed Papers*, pp. 177–186. Springer, 2010.

Francisco M Castro, Manuel J Marín-Jiménez, Nicolás Guil, Cordelia Schmid, and Karteek Alahari. End-to-end incremental learning. In *Proceedings of the European conference on computer vision (ECCV)*, pp. 233–248, 2018.

George Cazenavette, Tongzhou Wang, Antonio Torralba, Alexei A Efros, and Jun-Yan Zhu. Dataset distillation by matching training trajectories. In *Proceedings of the IEEE/CVF Conference on Computer Vision and Pattern Recognition (CVPR)*, pp. 4750–4759, 2022.

Yutian Chen, Max Welling, and Alex Smola. Super-samples from kernel herding. In *Proceedings of the Twenty-Sixth Conference on Uncertainty in Artificial Intelligence*, pp. 109–116, 2010.

Yeseul Cho, Baekrok Shin, Changmin Kang, and Chulhee Yun. Lightweight dataset pruning without full training via example difficulty and prediction uncertainty. In *Forty-second International Conference on Machine Learning (ICML)*, 2025.

Line H. Clemmensen and Rune D. Kjærsgaard. Data representativity for machine learning and ai systems. *arXiv preprint arXiv:2203.04706*, Mar 2022. URL `https://arxiv.org/abs/2203.04706`.

C Coleman, C Yeh, S Mussmann, B Mirzasoleiman, P Bailis, P Liang, J Leskovec, and M Zaharia. Selection via proxy: Efficient data selection for deep learning. In *International Conference on Learning Representations (ICLR)*, 2020.

Vitaly Feldman and Chiyuan Zhang. What neural networks memorize and why: Discovering the long tail via influence estimation. *Advances in Neural Information Processing Systems (NeurIPS)*, 33:2881–2891, 2020.

Isha Garg and Kaushik Roy. Samples with low loss curvature improve data efficiency. In *Proceedings of the IEEE/CVF Conference on Computer Vision and Pattern Recognition (CVPR)*, pp. 20290–20300, 2023.

Chengcheng Guo, Bo Zhao, and Yanbing Bai. Deepcore: A comprehensive library for coreset selection in deep learning. In *International Conference on Database and Expert Systems Applications*, pp. 181–195. Springer, 2022.

Satoshi Hara, Atsushi Nitanda, and Takanori Maehara. Data cleansing for models trained with sgd. *Advances in Neural Information Processing Systems (NeurIPS)*, 32, 2019.

Kaiming He, Xiangyu Zhang, Shaoqing Ren, and Jian Sun. Deep residual learning for image recognition. In *Proceedings of the IEEE conference on computer vision and pattern recognition (CVPR)*, pp. 770–778, 2016.

Muyang He, Shuo Yang, Tiejun Huang, and Bo Zhao. Large-scale dataset pruning with dynamic uncertainty. In *Proceedings of the IEEE/CVF Conference on Computer Vision and Pattern Recognition (CVPR)*, pp. 7713–7722, 2024.

Gao Huang, Zhuang Liu, Laurens Van Der Maaten, and Kilian Q Weinberger. Densely connected convolutional networks. In *Proceedings of the IEEE conference on computer vision and pattern recognition (CVPR)*, pp. 4700–4708, 2017.

Andrew Ilyas, Sung Min Park, Logan Engstrom, Guillaume Leclerc, and Aleksander Madry. Datamodels: Predicting predictions from training data. In *Proceedings of the 39th International Conference on Machine Learning (ICML)*, 2022.

Rishabh Iyer, Ninad Khargoankar, Jeff Bilmes, and Himanshu Asanani. Submodular combinatorial information measures with applications in machine learning. In *Algorithmic Learning Theory*, pp. 722–754. PMLR, 2021.

K Karthikeyan and Anders Søgaard. Revisiting methods for finding influential examples. *CoRR, abs/2111.04683*, 2021.

Krishnateja Killamsetty, Sivasubramanian Durga, Ganesh Ramakrishnan, Abir De, and Rishabh Iyer. Grad-match: Gradient matching based data subset selection for efficient deep model training. In *International Conference on Machine Learning (ICML)*, pp. 5464–5474. PMLR, 2021a.

Krishnateja Killamsetty, Durga Sivasubramanian, Ganesh Ramakrishnan, and Rishabh Iyer. Glister: Generalization based data subset selection for efficient and robust learning. In *Proceedings of the AAAI Conference on Artificial Intelligence*, volume 35, pp. 8110–8118, 2021b.

Pang Wei Koh and Percy Liang. Understanding black-box predictions via influence functions. In *International Conference on Machine Learning (ICML)*, pp. 1885–1894. PMLR, 2017.

Alex Krizhevsky, Vinod Nair, and Geoffrey Hinton. Cifar-100 (canadian institute for advanced research). *URL http://www. cs. toronto. edu/kriz/cifar. html*, 2009.

Adyasha Maharana, Prateek Yadav, and Mohit Bansal. D2 pruning: Message passing for balancing diversity and difficulty in data pruning. In *The Twelfth International Conference on Learning Representations (ICLR)*, 2024.

Katerina Margatina, Giorgos Vernikos, Loïc Barrault, and Nikolaos Aletras. Active learning by acquiring contrastive examples. In *Proceedings of the 2021 Conference on Empirical Methods in Natural Language Processing (EMNLP)*, pp. 650–663, 2021.

Baharan Mirzasoleiman, Jeff Bilmes, and Jure Leskovec. Coresets for data-efficient training of machine learning models. In *International Conference on Machine Learning (ICML)*, pp. 6950–6960. PMLR, 2020.

Byunggook Na, Jisoo Mok, Hyeokjun Choe, and Sungroh Yoon. Accelerating neural architecture search via proxy data. In *Proceedings of the Thirtieth International Joint Conference on Artificial Intelligence, IJCAI-21*. International Joint Conferences on Artificial Intelligence Organization, 2021.

Sung Min Park, Kristian Georgiev, Andrew Ilyas, Guillaume Leclerc, and Aleksander Madry. Trak: attributing model behavior at scale. In *Proceedings of the 40th International Conference on Machine Learning (ICML)*, pp. 27074–27113, 2023.

Mansheej Paul, Surya Ganguli, and Gintare Karolina Dziugaite. Deep learning on a data diet: Finding important examples early in training. *Advances in neural information processing systems (NeurIPS)*, 34: 20596–20607, 2021.

Karl Pearson. Vii. note on regression and inheritance in the case of two parents. *proceedings of the royal society of London*, 58(347-352):240–242, 1895.

Geoff Pleiss, Tianyi Zhang, Ethan Elenberg, and Kilian Q Weinberger. Identifying mislabeled data using the area under the margin ranking. *Advances in Neural Information Processing Systems (NeurIPS)*, 33: 17044–17056, 2020.

Garima Pruthi, Frederick Liu, Satyen Kale, and Mukund Sundararajan. Estimating training data influence by tracing gradient descent. *Advances in Neural Information Processing Systems (NeurIPS)*, 33:19920–19930, 2020.

Sylvestre-Alvise Rebuffi, Alexander Kolesnikov, Georg Sperl, and Christoph H Lampert. icarl: Incremental classifier and representation learning. In *Proceedings of the IEEE conference on Computer Vision and Pattern Recognition (CVPR)*, pp. 2001–2010, 2017.

Olga Russakovsky, Jia Deng, Hao Su, Jonathan Krause, Sanjeev Satheesh, Sean Ma, Zhiheng Huang, Andrej Karpathy, Aditya Khosla, Michael Bernstein, et al. Imagenet large scale visual recognition challenge. *International journal of computer vision*, 115:211–252, 2015.

Andrea Schioppa, Polina Zablotskaia, David Vilar, and Artem Sokolov. Scaling up influence functions. In *Proceedings of the AAAI Conference on Artificial Intelligence*, volume 36, pp. 8179–8186, 2022.

Ozan Sener and Silvio Savarese. Active learning for convolutional neural networks: A core-set approach. In *International Conference on Learning Representations (ICLR)*, 2018.

Jae-hun Shim, Kyeongbo Kong, and Suk-Ju Kang. Core-set sampling for efficient neural architecture search. *arXiv preprint arXiv:2107.06869*, 2021.

Karen Simonyan and Andrew Zisserman. Very deep convolutional networks for large-scale image recognition. *arXiv preprint arXiv:1409.1556*, 2014.

Charles Spearman. The proof and measurement of association between two things. *The American Journal of Psychology*, 15(1):72–101, 1904. doi: 10.2307/1412159. URL `https://www.jstor.org/stable/1412159`.

Ilya Sutskever, James Martens, George Dahl, and Geoffrey Hinton. On the importance of initialization and momentum in deep learning. In *International conference on machine learning (ICML)*, pp. 1139–1147. PMLR, 2013.

Mariya Toneva, Alessandro Sordoni, Remi Tachet des Combes, Adam Trischler, Yoshua Bengio, and Geoffrey J Gordon. An empirical study of example forgetting during deep neural network learning. In *International Conference on Learning Representations (ICLR)*, 2018.

Duco Veen, Jan C. Grutters, Matthias F. M. F. Veta, Max A. Viergever, and Josien P. W. Pluim. The data representativeness criterion: Predicting the performance of supervised classification based on data set similarity. *PLOS ONE*, 15(8):e0237009, 2020. doi: 10.1371/journal.pone.0237009.

Mike Wojnowicz, Ben Cruz, Xuan Zhao, Brian Wallace, Matt Wolff, Jay Luan, and Caleb Crable. "influence sketching": Finding influential samples in large-scale regressions. In *2016 IEEE International Conference on Big Data (Big Data)*, pp. 3601–3612. IEEE, 2016.

Xiaobo Xia, Jiale Liu, Jun Yu, Xu Shen, Bo Han, and Tongliang Liu. Moderate coreset: A universal method of data selection for real-world data-efficient deep learning. In *The Eleventh International Conference on Learning Representations (ICLR)*, 2022.

Xiaobo Xia, Jiale Liu, Shaokun Zhang, Qingyun Wu, Hongxin Wei, and Tongliang Liu. Refined coreset selection: Towards minimal coreset size under model performance constraints. In *Forty-first International Conference on Machine Learning (ICML)*, 2024.

Shuo Yang, Zhe Cao, Sheng Guo, Ruiheng Zhang, Ping Luo, Shengping Zhang, and Liqiang Nie. Mind the boundary: Coreset selection via reconstructing the decision boundary. In *Forty-first International Conference on Machine Learning (ICML)*, 2024.

Wei Yang. Pytorch-classification. `https://github.com/bearpaw/pytorch-classification`, 2017.

Chih-Kuan Yeh, Joon Kim, Ian En-Hsu Yen, and Pradeep K Ravikumar. Representer point selection for explaining deep neural networks. *Advances in neural information processing systems (NeurIPS)*, 31, 2018.

Mengying Zhang, Mary L. Li, Tesi Liu, Yong Yu, and Zhi-Hua Zhou. Deep active learning by leveraging training dynamics. In *Advances in Neural Information Processing Systems 35 (NeurIPS 2022)*, pp. 14737–14750, 2022.

Xin Zhang, Jiawei Du, Yunsong Li, Weiying Xie, and Joey Tianyi Zhou. Spanning training progress: Temporal dual-depth scoring (tdds) for enhanced dataset pruning. In *Proceedings of the IEEE/CVF Conference on Computer Vision and Pattern Recognition (CVPR)*, pp. 26223–26232, 2024.

Haizhong Zheng, Rui Liu, Fan Lai, and Atul Prakash. Coverage-centric coreset selection for high pruning rates. In *The Eleventh International Conference on Learning Representations (ICLR)*, 2022.

A CLD-Coreset Selection Algorithm

For completeness, we provide the full pseudocode for the coreset selection procedure described in Section 4.1. This algorithm computes per-class CLD scores by correlating each training sample's loss trajectory with the corresponding class-specific validation trajectory, and selects a fixed number of top-scoring samples per class to form a class-balanced coreset.

Algorithm 1: Coreset Selection Using CLD (Per-Class)

Input: Training set $\mathbf{S} = \{\vec{z}_m\}_{m=1}^{N}$, Validation set $\mathbf{V} = \{\vec{q}_j\}_{j=1}^{Q}$, Class budgets $\{k_c\}_{c=1}^{C}$ with $k = \sum_{c=1}^{C} k_c$, Epochs T, Initial params $\theta_{\mathbf{S}}^{0}$, Loss ℓ, Optimizer $\mathcal{A}$, Hyperparameters λ

Output: Coreset $\mathbf{C}$ of size k

for $t \leftarrow 1$ **to** T **do**
  $\theta_{\mathbf{S}}^{t} \leftarrow \mathcal{A}(\theta_{\mathbf{S}}^{t-1}, \mathbf{S}, \lambda)$ `// update model`
  for $m \leftarrow 1$ **to** N **do**
    Store $\ell(\theta_{\mathbf{S}}^{t}, \vec{z}_m)$ `// record train loss`
  for $j \leftarrow 1$ **to** Q **do**
    Store $\ell(\theta_{\mathbf{S}}^{t}, \vec{q}_j)$ `// record val loss`
for $m \leftarrow 1$ **to** N **do**
  $\vec{\Delta}(\vec{z}_m) \leftarrow \left[\ell(\theta_{\mathbf{S}}^{t}, \vec{z}_m) - \ell(\theta_{\mathbf{S}}^{t-1}, \vec{z}_m)\right]_{t=1}^{T}$
for $j \leftarrow 1$ **to** Q **do**
  $\vec{\Delta}(\vec{q}_j) \leftarrow \left[\ell(\theta_{\mathbf{S}}^{t}, \vec{q}_j) - \ell(\theta_{\mathbf{S}}^{t-1}, \vec{q}_j)\right]_{t=1}^{T}$
for $c \leftarrow 1$ **to** C **do**
  $\mathbf{S}_c \leftarrow \{\vec{z}_m \in \mathbf{S} : y_m = c\}$;
  $\mathbf{V}_c \leftarrow \{\vec{q}_j \in \mathbf{V} : y_j = c\}$;
  $\vec{\Delta}'_{\mathbf{V},c} \leftarrow \frac{1}{|\mathbf{V}_c|} \sum_{\vec{q}_j \in \mathbf{V}_c} \vec{\Delta}(\vec{q}_j)$;
  foreach $\vec{z}_m \in \mathbf{S}_c$ **do**
    $\texttt{CLD}(\vec{z}_m) \leftarrow \rho\big(\vec{\Delta}(\vec{z}_m),\, \vec{\Delta}'_{\mathbf{V},c}\big)$
  $\mathbf{C}_c \leftarrow$ top-k_c elements of $\mathbf{S}_c$ by $\texttt{CLD}(\vec{z}_m)$;
$\mathbf{C} \leftarrow \bigcup_{c=1}^{C} \mathbf{C}_c$;
return $\mathbf{C}$

B Detailed Theoretical Framework

In this appendix, we provide the complete theoretical framework supporting the results stated in Section 5. We first outline the detailed lemmas establishing gradient alignment and approximation properties of CLD-selected coresets. We then conclude with a full proof of the convergence guarantee presented in Theorem 1.

B.1 Supporting Lemmas for Theorem 1

Lemma 1 (High CLD Implies Gradient Alignment)**.** *Consider a training sample $\vec{z}_m \in \mathbf{S}$ with $\texttt{CLD}(\vec{z}_m) = \rho\big(\vec{\Delta}(\vec{z}_m), \vec{\Delta}'_{\mathbf{V}}\big) \geq 1 - \epsilon$ for some small $\epsilon > 0$. Let $\theta_{\mathbf{S}}^{t}$ be the parameters obtained by running algorithm $\mathcal{A}$ on $\mathbf{S}$ for t iterations. Let $\delta\theta^{t-1} := \theta_{\mathbf{S}}^{t} - \theta_{\mathbf{S}}^{t-1}$ be the parameter update at step t.*

Suppose the learning algorithm is run for a sufficiently large number of iterations T. Assume the sequence of parameter updates $\{\delta\theta^{t-1}\}_{t=1}^{T}$ is sufficiently varied. This means the updates are not persistently orthogonal to any fixed non-zero vector direction in the relevant parameter subspace.

Then, for most training steps t where $G_{\mathbf{V}}(\theta_{\mathbf{S}}^{t}) \neq 0$, the sample gradient $\nabla_\theta \ell(\theta_{\mathbf{S}}^{t}, \vec{z}_m)$ and the validation gradient $G_{\mathbf{V}}(\theta_{\mathbf{S}}^{t})$ are well-aligned:

$$\cos\left(\angle\left(\nabla_\theta \ell(\theta_{\mathbf{S}}^{t}, \vec{z}_m), G_{\mathbf{V}}(\theta_{\mathbf{S}}^{t})\right)\right) \geq 1 - \epsilon'_t, \tag{17}$$

where $\epsilon'_t \to 0$ *as* $\epsilon \to 0$.

Proof. We first analyze the idealized case where the correlation is perfect ($\epsilon = 0$) and the underlying approximations hold exactly, and then argue by continuity.

Assume the first-order Taylor expansions are exact for the loss changes:

$$\left(\vec{\Delta}(\vec{z}_m)\right)_t = \ell(\theta^t_{\mathbf{S}}, \vec{z}_m) - \ell(\theta^{t-1}_{\mathbf{S}}, \vec{z}_m) \approx \langle \nabla_\theta \ell(\theta^{t-1}_{\mathbf{S}}, \vec{z}_m), \delta\theta^{t-1} \rangle = x_t, \tag{18}$$

$$(\vec{\Delta}'_{\mathbf{V}})_t = \frac{1}{Q} \sum_{j=1}^{Q} \left(\ell(\theta^t_{\mathbf{S}}, \vec{q}_j) - \ell(\theta^{t-1}_{\mathbf{S}}, \vec{q}_j)\right) \approx \langle G_{\mathbf{V}}(\theta^{t-1}_{\mathbf{S}}), \delta\theta^{t-1} \rangle = y_t. \tag{19}$$

Assume perfect correlation $\rho(\vec{x}, \vec{y}) = 1$.
This implies an exact positive linear relationship $x_t = c\, y_t + K'$ for all t, where $c = \sigma_x/\sigma_y > 0$ and $K' = \overline{x} - c\,\overline{y}$.
Substituting the definitions of x_t and y_t:

$$\langle \nabla_\theta \ell(\theta^{t-1}_{\mathbf{S}}, \vec{z}_m), \delta\theta^{t-1} \rangle = c\, \langle G_{\mathbf{V}}(\theta^{t-1}_{\mathbf{S}}), \delta\theta^{t-1} \rangle + K'. \tag{20}$$

Rearranging yields:

$$\langle \nabla_\theta \ell(\theta^{t-1}_{\mathbf{S}}, \vec{z}_m) - c\, G_{\mathbf{V}}(\theta^{t-1}_{\mathbf{S}}), \delta\theta^{t-1} \rangle = K'. \tag{21}$$

Since the mean of the loss trajectory will be smaller compared to the variance of the terms (losses eventually reduce to 0), it is reasonable to assume $K' \approx 0$.
Thus, for $t = 1, \ldots, T$:

$$\langle \nabla_\theta \ell(\theta^{t-1}_{\mathbf{S}}, \vec{z}_m) - c\, G_{\mathbf{V}}(\theta^{t-1}_{\mathbf{S}}), \delta\theta^{t-1} \rangle = 0. \tag{22}$$

Let $\vec{w}_{t-1} \coloneqq \nabla_\theta \ell(\theta^{t-1}_{\mathbf{S}}, \vec{z}_m) - c\, G_{\mathbf{V}}(\theta^{t-1}_{\mathbf{S}})$.
The vector $\vec{w}_{t-1}$ is exactly orthogonal to the update direction $\delta\theta^{t-1}$ at each step t.

Now, invoke the assumption that the sequence of updates $\{\delta\theta^{t-1}\}_{t=1}^T$ is sufficiently varied.
This means the updates are not persistently orthogonal to any fixed non-zero direction $\vec{w}_{t-1}$.
If $\vec{w}_{t-1}$ were non-zero, the variation in updates would eventually yield a $\delta\theta^{t-1}$ such that $\langle \vec{w}_{t-1}, \delta\theta^{t-1} \rangle \neq 0$.
Since the inner product is exactly zero for all t in our idealized case, the only possibility consistent with the sufficient variation assumption is that $\vec{w}_{t-1}$ must be the zero vector. Thus:

$$\vec{w}_{t-1} = \nabla_\theta \ell(\theta^{t-1}_{\mathbf{S}}, \vec{z}_m) - c\, G_{\mathbf{V}}(\theta^{t-1}_{\mathbf{S}}) = \vec{0}. \tag{23}$$

This signifies that the sample gradient is exactly a positive scalar multiple ($c > 0$) of the validation gradient:

$$\nabla_\theta \ell(\theta^{t-1}_{\mathbf{S}}, \vec{z}_m) = c\, G_{\mathbf{V}}(\theta^{t-1}_{\mathbf{S}}). \tag{24}$$

Consequently, the vectors are perfectly collinear and point in the same direction (assuming $G_{\mathbf{V}}(\theta^{t-1}_{\mathbf{S}}) \neq 0$).
The angle γ_{t-1} between them is exactly 0. Therefore, in this idealized case:

$$\cos(\gamma_{t-1}) = \cos\left(\angle\left(\nabla_\theta \ell(\theta^{t-1}_{\mathbf{S}}, \vec{z}_m), G_{\mathbf{V}}(\theta^{t-1}_{\mathbf{S}})\right)\right) = 1. \tag{25}$$

This derivation holds under the ideal conditions ($\epsilon = 0$, exact Taylor approx., $K' = 0$).
Since the involved operations are continuous, when the conditions are only approximately met (i.e., $\rho \geq 1 - \epsilon$ with $\epsilon \to 0$, Taylor approx. is good, K' is small), the resulting cosine similarity will be close to 1.
We express this conclusion as

$$\cos(\gamma_{t-1}) \geq 1 - \epsilon'_{t-1}, \tag{26}$$

where the error $\epsilon'_{t-1} \to 0$ as $\epsilon \to 0$.
Assuming this alignment holds for most steps t (implying alignment at step t relies on properties at $t-1$), the lemma statement follows. □

Remark 2 (On Update Sequence Variation)**.** *The assumption regarding the update sequence* $\{\delta\theta^{t-1}\}$ *is that it exhibits enough variation over the trajectory to ensure that no fixed non-zero vector can remain orthogonal to all updates. This property is weaker than requiring the updates to span the entire parameter space, but it is sufficient for the argument. It essentially prevents the gradient difference vector from hiding in a direction that the optimization process never explores. Stochastic optimization methods accumulating updates over many iterations (large* T*) are often expected to satisfy this sufficient variation condition.*

Lemma 2 (Stability of Gradient Alignment)**.** *Suppose the conditions in Theorem 1 hold: specifically, L-smoothness and bounded gradients ($\|\nabla_\theta \ell(\theta, \vec{z})\|_2 \leq B$ for all $\vec{z}$). Consider a coreset $\mathbf{C}$ constructed by selecting samples with high* CLD *scores:*

$$\mathbf{C} = \{\vec{z}_m \in \mathbf{S} : \texttt{CLD}(\vec{z}_m) \geq 1 - \epsilon\}, \quad \textit{with} \quad |\mathbf{C}| = k\ ,\ \epsilon > 0,\ \epsilon \to 0. \tag{27}$$

Assume that during training, the difference between the parameter trajectories satisfies $\|\theta^t_{\mathbf{C}} - \theta^t_{\mathbf{S}}\|_2 = \|\delta_t\|_2$ at step t.

Then, for each sample $\vec{z}_m \in \mathbf{C}$, the cosine similarity between its gradient and the average validation gradient at step t is lower bounded by

$$\cos\left(\angle\left(\nabla_\theta \ell(\theta^t_{\mathbf{C}}, \vec{z}_m), G_{\mathbf{V}}(\theta^t_{\mathbf{C}})\right)\right) \geq 1 - \kappa, \tag{28}$$

where $\kappa = \epsilon'_t + \frac{4L}{B}\|\delta_t\|_2 + \frac{3L^2}{B^2}\|\delta_t\|_2^2$, and $\epsilon'_t \to 0$ as $\epsilon \to 0$.

Proof. Let $\omega_m = \nabla_\theta \ell(\theta^t_{\mathbf{C}}, \vec{z}_m) - \nabla_\theta \ell(\theta^t_{\mathbf{S}}, \vec{z}_m)$ and $\omega_{\mathbf{V}} = G_{\mathbf{V}}(\theta^t_{\mathbf{C}}) - G_{\mathbf{V}}(\theta^t_{\mathbf{S}})$ denote the deviations between gradients evaluated on the coreset trajectory and the full dataset trajectory.

By L-smoothness of $\ell(\cdot, \vec{z}_m)$ and of the validation-average loss $\hat{R}_{\mathbf{V}}(\theta) \coloneqq \frac{1}{Q}\sum_{j=1}^{Q} \ell(\theta, \vec{q}_j)$, we have:

$$\|\omega_m\|_2 \leq L\|\delta_t\|_2, \tag{29}$$
$$\|\omega_{\mathbf{V}}\|_2 \leq L\|\delta_t\|_2. \tag{30}$$

Expanding the inner product:

$$\langle \nabla_\theta \ell(\theta^t_{\mathbf{C}}, \vec{z}_m), G_{\mathbf{V}}(\theta^t_{\mathbf{C}})\rangle = \langle \nabla_\theta \ell(\theta^t_{\mathbf{S}}, \vec{z}_m) + \omega_m, G_{\mathbf{V}}(\theta^t_{\mathbf{S}}) + \omega_{\mathbf{V}}\rangle \tag{31}$$
$$= \langle \nabla_\theta \ell(\theta^t_{\mathbf{S}}, \vec{z}_m), G_{\mathbf{V}}(\theta^t_{\mathbf{S}})\rangle + \langle \omega_m, G_{\mathbf{V}}(\theta^t_{\mathbf{S}})\rangle + \langle \nabla_\theta \ell(\theta^t_{\mathbf{S}}, \vec{z}_m), \omega_{\mathbf{V}}\rangle + \langle \omega_m, \omega_{\mathbf{V}}\rangle. \tag{32}$$

Applying Cauchy–Schwarz inequality and the bounded gradient norm $\|\nabla_\theta \ell(\theta, \vec{z})\|_2 \leq B$, we have:

$$\langle \omega_m, G_{\mathbf{V}}(\theta^t_{\mathbf{S}})\rangle \geq -\|\omega_m\|_2 \left\|G_{\mathbf{V}}(\theta^t_{\mathbf{S}})\right\|_2 \geq -LB\|\delta_t\|_2, \tag{33}$$
$$\langle \nabla_\theta \ell(\theta^t_{\mathbf{S}}, \vec{z}_m), \omega_{\mathbf{V}}\rangle \geq -\left\|\nabla_\theta \ell(\theta^t_{\mathbf{S}}, \vec{z}_m)\right\|_2 \|\omega_{\mathbf{V}}\|_2 \geq -LB\|\delta_t\|_2, \tag{34}$$
$$\langle \omega_m, \omega_{\mathbf{V}}\rangle \geq -\|\omega_m\|_2 \|\omega_{\mathbf{V}}\|_2 \geq -L^2\|\delta_t\|_2^2. \tag{35}$$

Thus,

$$\langle \nabla_\theta \ell(\theta^t_{\mathbf{C}}, \vec{z}_m), G_{\mathbf{V}}(\theta^t_{\mathbf{C}})\rangle \geq \langle \nabla_\theta \ell(\theta^t_{\mathbf{S}}, \vec{z}_m), G_{\mathbf{V}}(\theta^t_{\mathbf{S}})\rangle - 2LB\|\delta_t\|_2 - L^2\|\delta_t\|_2^2. \tag{36}$$

The denominator is upper bounded by:

$$\left\|\nabla_\theta \ell(\theta^t_{\mathbf{C}}, \vec{z}_m)\right\|_2 \left\|G_{\mathbf{V}}(\theta^t_{\mathbf{C}})\right\|_2 \leq (B + L\|\delta_t\|_2)^2. \tag{37}$$

Combining this result with Lemma 1, we can conclude:

$$\cos\left(\angle\left(\nabla_\theta \ell(\theta^t_{\mathbf{C}}, \vec{z}_m), G_{\mathbf{V}}(\theta^t_{\mathbf{C}})\right)\right) \geq 1 - \left(\epsilon'_t + \frac{4L}{B}\|\delta_t\|_2 + \frac{3L^2}{B^2}\|\delta_t\|_2^2\right) = 1 - \kappa, \tag{38}$$

where ϵ'_t captures the initial alignment error when training on $\mathbf{S}$. This completes the proof. □

Remark 3. *Lemma 2 shows that if a sample's gradient is well-aligned with the validation gradient during training on the full dataset (i.e., ϵ'_t is small), then this alignment is preserved when training on a coreset $\mathbf{C}$, as long as the parameter trajectories $\theta^t_{\mathbf{S}}$ and $\theta^t_{\mathbf{C}}$ remain close. The degradation in alignment is bounded by terms that are linear and quadratic in $\|\delta_t\|_2$. Thus, as long as the coreset trajectory stays near the full dataset trajectory, the generalization-relevant properties captured by* CLD *remain stable. This stability is crucial for ensuring that* CLD*-based coresets maintain the training dynamics of the full dataset.*

Remark 4 (Influence of Coreset Size on κ)**.** *It is important to explicitly consider how the coreset size $k = |\mathbf{C}|$ (as specified in Lemma 2) influences the components of $\kappa = \epsilon'_t + \frac{4L}{B}\|\delta_t\|_2 + \frac{3L^2}{B^2}\|\delta_t\|_2^2$.*

- *The term ϵ'_t, representing the initial alignment error derived from Lemma 1, is affected by k. A smaller coreset size k allows for a more stringent selection criterion for samples based on their* `CLD` *scores. Specifically, one can choose only samples with* $\texttt{CLD}(\vec{z}_m)$ *very close to* 1*, which corresponds to a smaller ϵ in the selection rule* $\texttt{CLD}(\vec{z}_m) \geq 1 - \epsilon$ *(from Theorem 1 and Lemma 2). A smaller ϵ naturally leads to a smaller ϵ'_t.*
- *Conversely, the terms in κ that depend on $\|\delta_t\|_2 = \|\theta^t_{\mathbf{C}} - \theta^t_{\mathbf{S}}\|_2$ (the deviation between coreset and full-data parameter trajectories) are also influenced by k. While a smaller k allows for higher individual sample quality, a very small k might result in a coreset that is less representative of the full dataset $\mathbf{S}$. This reduced representativeness can lead to a larger divergence $\|\delta_t\|_2$ during training, as the optimization trajectory on the small coreset may differ more substantially from that on the full data. An increase in $\|\delta_t\|_2$ would, in turn, increase the overall value of κ.*

Therefore, the selection of an appropriate coreset size k involves an inherent trade-off. A smaller k can be beneficial for the ϵ'_t component of κ by enabling the selection of higher-quality samples. However, if k is too small, it could adversely affect the components of κ related to $\|\delta_t\|_2$ by making the coreset insufficiently representative. The stability discussed in Remark 3 relies on $\|\delta_t\|_2$ remaining small, highlighting the importance of k being chosen to adequately approximate the full dataset's training dynamics while leveraging the benefits of high `CLD` *scores.*

Lemma 3 (Subset-Gradient Approximation)**.** *Suppose the conditions in Theorem 1 hold, including L-smoothness, bounded gradients, and validation representativeness as described in Section 5.*

Define the average coreset gradient at step t as

$$\gamma^t_{\mathbf{C}} = \frac{1}{|\mathbf{C}|}\sum_{m\in\mathbf{C}} \nabla_\theta \ell(\theta^t_{\mathbf{C}}, \vec{z}_m). \tag{39}$$

Then, for every training step t, we have

$$\left\|\gamma^t_{\mathbf{C}} - \nabla_\theta R_{\mathbf{D}}(\theta^t_{\mathbf{C}})\right\|_2 \leq B\sqrt{2\kappa} + \delta, \tag{40}$$

where κ captures the alignment error and satisfies $\kappa \to 0$ as $\epsilon \to 0$.

Proof. We decompose the error using the triangle inequality:

$$\left\|\gamma^t_{\mathbf{C}} - \nabla_\theta R_{\mathbf{D}}(\theta^t_{\mathbf{C}})\right\|_2 \leq \left\|\gamma^t_{\mathbf{C}} - G_{\mathbf{V}}(\theta^t_{\mathbf{C}})\right\|_2 + \left\|G_{\mathbf{V}}(\theta^t_{\mathbf{C}}) - \nabla_\theta R_{\mathbf{D}}(\theta^t_{\mathbf{C}})\right\|_2. \tag{41}$$

The second term $\|G_{\mathbf{V}}(\theta^t_{\mathbf{C}}) - \nabla_\theta R_{\mathbf{D}}(\theta^t_{\mathbf{C}})\|_2$ is bounded by δ by the validation representativeness assumption. To bound the first term $\|\gamma^t_{\mathbf{C}} - G_{\mathbf{V}}(\theta^t_{\mathbf{C}})\|_2$, we apply Jensen's inequality:

$$\left\|\gamma^t_{\mathbf{C}} - G_{\mathbf{V}}(\theta^t_{\mathbf{C}})\right\|_2^2 = \left\|\frac{1}{|\mathbf{C}|}\sum_{m\in\mathbf{C}}\left(\nabla_\theta \ell(\theta^t_{\mathbf{C}}, \vec{z}_m) - G_{\mathbf{V}}(\theta^t_{\mathbf{C}})\right)\right\|^2 \tag{42}$$

$$\leq \frac{1}{|\mathbf{C}|}\sum_{m\in\mathbf{C}}\left\|\nabla_\theta \ell(\theta^t_{\mathbf{C}}, \vec{z}_m) - G_{\mathbf{V}}(\theta^t_{\mathbf{C}})\right\|_2^2. \tag{43}$$

Define φ^t_m as the angle between $\nabla_\theta \ell(\theta^t_{\mathbf{C}}, \vec{z}_m)$ and $G_{\mathbf{V}}(\theta^t_{\mathbf{C}})$. By Lemma 2, we have $\cos\varphi^t_m \geq 1 - \kappa$ for all m. Expanding the squared distance:

$$\left\|\nabla_\theta \ell(\theta^t_{\mathbf{C}}, \vec{z}_m) - G_{\mathbf{V}}(\theta^t_{\mathbf{C}})\right\|_2^2 = \left\|\nabla_\theta \ell(\theta^t_{\mathbf{C}}, \vec{z}_m)\right\|_2^2 + \left\|G_{\mathbf{V}}(\theta^t_{\mathbf{C}})\right\|_2^2 - 2\langle \nabla_\theta \ell(\theta^t_{\mathbf{C}}, \vec{z}_m), G_{\mathbf{V}}(\theta^t_{\mathbf{C}})\rangle \tag{44}$$

$$= \left\|\nabla_\theta \ell(\theta^t_{\mathbf{C}}, \vec{z}_m)\right\|_2{}^2 + \left\|G_{\mathbf{V}}(\theta^t_{\mathbf{C}})\right\|_2^2 - 2\left\|\nabla_\theta \ell(\theta^t_{\mathbf{C}}, \vec{z}_m)\right\|_2 \left\|G_{\mathbf{V}}(\theta^t_{\mathbf{C}})\right\|_2 \cos\varphi^t_m. \tag{45}$$

Since $\|\nabla_\theta \ell(\theta^t_{\mathbf{C}}, \vec{z}_m)\|_2, \|G_{\mathbf{V}}(\theta^t_{\mathbf{C}})\|_2 \leq B$ and $\cos\varphi^t_m \geq 1-\kappa$, we have

$$\left\|\nabla_\theta \ell(\theta^t_{\mathbf{C}}, \vec{z}_m) - G_{\mathbf{V}}(\theta^t_{\mathbf{C}})\right\|_2^2 \leq 2B^2\kappa. \tag{46}$$

Substituting back into the Jensen bound,

$$\left\|\gamma^t_{\mathbf{C}} - G_{\mathbf{V}}(\theta^t_{\mathbf{C}})\right\|_2^2 \leq 2B^2\kappa. \tag{47}$$

Taking square roots gives

$$\left\|\gamma^t_{\mathbf{C}} - G_{\mathbf{V}}(\theta^t_{\mathbf{C}})\right\|_2 \leq B\sqrt{2\kappa}. \tag{48}$$

Thus, combining the two bounds,

$$\left\|\gamma^t_{\mathbf{C}} - \nabla_\theta R_{\mathbf{D}}(\theta^t_{\mathbf{C}})\right\|_2 \leq B\sqrt{2\kappa} + \delta, \tag{49}$$

as claimed. □

Remark 5. *Lemma 3 shows that under mild conditions, the average gradient computed over a coreset selected based on* `CLD` *remains close to the true risk gradient throughout training. The deviation is controlled by two sources: the alignment error κ arising from the selection of high-*`CLD` *samples, and the validation approximation error δ due to finite sample size. Consequently, optimization over* `CLD`*-coresets closely tracks the gradient flow of the full dataset, ensuring that convergence and generalization properties are preserved. This result is crucial for connecting loss trajectory dynamics with practical coreset construction.*

B.2 Proof for Theorem 1

Proof. Define

$$R_t \coloneqq R_{\mathbf{D}}(\theta^t_{\mathbf{C}}), \qquad G_t \coloneqq \nabla_\theta R_{\mathbf{D}}(\theta^t_{\mathbf{C}}), \qquad \gamma^t_{\mathbf{C}} \coloneqq \frac{1}{|\mathbf{C}|}\sum_{m\in\mathbf{C}} \nabla_\theta \ell(\theta^t_{\mathbf{C}}, \vec{z}_m). \tag{50}$$

By L-smoothness of $\ell(\cdot)$, and in extension $R_{\mathbf{D}}(\cdot)$, and $\eta \leq 1/L$,

$$R_{t+1} \leq R_t + \langle G_t, \theta^{t+1}_{\mathbf{C}} - \theta^t_{\mathbf{C}}\rangle + \frac{L}{2}\left\|\theta^{t+1}_{\mathbf{C}} - \theta^t_{\mathbf{C}}\right\|_2^2. \tag{51}$$

Substituting the model update $\theta^{t+1}_{\mathbf{C}} - \theta^t_{\mathbf{C}} = -\eta\gamma^t_{\mathbf{C}}$:

$$R_{t+1} \leq R_t - \eta\langle G_t, \gamma^t_{\mathbf{C}}\rangle + \frac{L\eta^2}{2}\left\|\gamma^t_{\mathbf{C}}\right\|_2^2. \tag{52}$$

Rearranging,

$$\eta\langle G_t, \gamma^t_{\mathbf{C}}\rangle \leq R_t - R_{t+1} + \frac{L\eta^2}{2}\left\|\gamma^t_{\mathbf{C}}\right\|_2^2. \tag{53}$$

Decomposing the inner product using the true gradient G_t we get,

$$\langle G_t, \gamma^t_{\mathbf{C}}\rangle = \langle G_t,\, G_t + (\gamma^t_{\mathbf{C}} - G_t)\rangle = \|G_t\|_2^2 + \langle G_t, \gamma^t_{\mathbf{C}} - G_t\rangle. \tag{54}$$

Substituting this back,

$$\eta\|G_t\|_2^2 \leq R_t - R_{t+1} - \eta\langle G_t, \gamma^t_{\mathbf{C}} - G_t\rangle + \frac{L\eta^2}{2}\left\|\gamma^t_{\mathbf{C}}\right\|_2^2. \tag{55}$$

Let $E_t = \|\gamma^t_{\mathbf{C}} - G_t\|_2$.
Lemma 3 under the stated assumptions gives the bound $E_t \leq B\sqrt{2\kappa} + \delta$.
By Cauchy–Schwarz inequality,

$$-\eta\langle G_t, \gamma^t_{\mathbf{C}} - G_t\rangle \;\leq\; \eta\|G_t\|_2\left\|\gamma^t_{\mathbf{C}} - G_t\right\|_2 = \eta\|G_t\|_2 E_t. \tag{56}$$

Young's inequality states that $ab \leq a^2/(2\gamma) + \gamma b^2/2, \quad \forall a, b \geq 0$ and $\gamma > 0$.
By using this inequality with $\gamma = 1$,

$$-\eta\langle G_t, \gamma_{\mathbf{C}}^t - G_t\rangle \;\leq\; \frac{\eta}{2}\,\|G_t\|_2^2 + \frac{\eta}{2}E_t^2. \tag{57}$$

Substituting this into the inequality in Equation (55),

$$\eta\,\|G_t\|_2^2 \leq R_t - R_{t+1} + \tfrac{\eta}{2}\,\|G_t\|_2^2 + \tfrac{\eta}{2}\,E_t^2 + \frac{L\eta^2}{2}\,\left\|\gamma_{\mathbf{C}}^t\right\|_2^2. \tag{58}$$

Since all gradients are bounded by B, their average $\|\gamma_{\mathbf{C}}^t\|_2$ is also bounded by B.

$$\therefore \frac{\eta}{2}\,\|G_t\|_2^2 \;\leq\; R_t - R_{t+1} + \frac{\eta}{2}\,E_t^2 + \frac{L\eta^2}{2}\,B^2. \tag{59}$$

Summing from $t = 0$ to $T - 1$:

$$\frac{\eta}{2}\sum_{t=0}^{T-1}\|G_t\|_2^2 \;\leq\; (R_0 - R_T) + \sum_{t=0}^{T-1}\left(\frac{\eta}{2}\,E_t^2 + \frac{L\eta^2}{2}\,B^2\right). \tag{60}$$

Let $R_{\text{inf}} = \inf_\theta R_{\mathbf{D}}(\theta)$. Then $R_0 - R_T \leq R_0 - R_{\text{inf}}$. Substituting the bound $E_t \leq B\sqrt{2\kappa} + \delta$:

$$\frac{\eta}{2}\sum_{t=0}^{T-1}\|G_t\|_2^2 \;\leq\; R_{\mathbf{D}}(\theta_{\mathbf{C}}^0) - R_{\text{inf}} + T\frac{\eta}{2}\,(B\sqrt{2\kappa} + \delta)^2 + T\frac{L\eta^2}{2}\,B^2. \tag{61}$$

The sum on the left is lower bounded by T times the minimum term, i.e., $\sum_{t=0}^{T-1}\|G_t\|_2^2 \geq T \cdot \min_{0\leq t<T}\|G_t\|_2^2$.

$$\therefore \frac{\eta T}{2}\min_{0\leq t<T}\|G_t\|_2^2 \;\leq\; R_{\mathbf{D}}(\theta_{\mathbf{C}}^0) - R_{\text{inf}} + T\frac{\eta}{2}\,(B\sqrt{2\kappa} + \delta)^2 + T\frac{L\eta^2}{2}\,B^2. \tag{62}$$

Since $\eta, T > 0$,

$$\min_{0\leq t<T}\|G_t\|_2^2 \leq \frac{2\big[R_{\mathbf{D}}(\theta_C^0) - R_{\text{inf}}\big]}{\eta T} + (B\sqrt{2\kappa} + \delta)^2 + L\eta B^2. \tag{63}$$

This proves the theorem. □

C Datasets, Models, and Experimental Details

We evaluate our method on two standard image classification benchmarks: CIFAR-100 (Krizhevsky et al., 2009) and ImageNet-1k (Russakovsky et al., 2015). CIFAR-100 consists of 50,000 training and 10,000 test images across 100 classes and is publicly available without licensing restrictions. For ImageNet-1k, we use the official release from `https://image-net.org/download.php`, which is provided under a standard academic research license and requires user agreement to the terms of access.

Architectures. Our experiments employ the following CNN backbones:

- **ResNet-18, ResNet-34, and ResNet-50** He et al. (2016) from `https://pytorch.org/vision/stable/models/resnet.html` (BSD-3-Clause license).
- **VGG-19 with batch normalization** Simonyan & Zisserman (2014) from `https://pytorch.org/vision/stable/models/vgg.html` (BSD-3-Clause license).
- **DenseNet-121** Huang et al. (2017) from `https://pytorch.org/vision/stable/models/densenet.html` (BSD-3-Clause license).

For baseline comparisons, we use the `DeepCore` library Guo et al. (2022) (`https://github.com/PatrickZH/DeepCore`), which provides standardized implementations of several coreset selection techniques and is licensed under MIT. All training and evaluation code was implemented in PyTorch; dependencies including torchvision are MIT/BSD licensed.

Training Setup for CIFAR-100. All networks were trained using SGD Bottou (2010) for 164 epochs with an initial learning rate of 0.1, decayed by a factor of 0.1 at epochs 81 and 121. Nesterov momentum Sutskever et al. (2013) with momentum 0.9 was used, along with weight decay 5×10^{-4}. Standard augmentations included resizing to 32×32, random cropping with padding $= 4$, random horizontal flips, and normalization.

Training Setup for ImageNet-1k. Training followed standard ImageNet protocols: all models were trained with SGD for 90 epochs, with a learning rate of 0.1 decayed by 0.1 at epochs 30 and 60. Nesterov momentum with coefficient 0.9 and weight decay 10^{-4} were used. Data augmentations included random resized cropping to 224×224, horizontal flipping, and normalization.

Reproducibility. No fine-tuning or additional regularization was applied to any method, including ours, ensuring fairness in coreset comparisons. All methods used the same validation split as the validation proxy, and the same train split as the full training set available for each seed when scoring training samples. Each experiment was repeated across 5 independent runs with distinct seeds; reported results reflect the mean and standard deviation.

All experiments were conducted on a private compute cluster with access to NVIDIA A40 GPUs (48 GB memory, 300W TDP). All training and evaluation runs were performed in full precision using PyTorch.

Results. Performance results for CIFAR-100 and ImageNet-1k coreset experiments are shown in Tables 2, 3, 4, and 5. Cross-architecture transferability results for `CLD` coresets, as discussed in Section 6, are shown in Table 6.

Table 2: Performance (top-1 accuracy) of score-based coreset methods on CIFAR100 trainsplit. The coresets were selected and finetuned on ResNet-18. The full trainset performance was $\mathbf{70.95 \pm 0.68}$. The mean accuracy over 5 runs, along with their standard deviation, is reported.

Coreset Sizes	Random	Herding	Forgetting	Cal	EL2N	Moderate	CCS(AUM)	$\mathbb{D}^2$-Pruning	**CLD (Ours)**
0.2%	3.66 ± 0.41	2.57 ± 0.52	3.52 ± 0.16	5.24 ± 0.41	3.9 ± 0.45	3.8 ± 0.47	4.1 ± 0.5	4.6 ± 0.52	**5.67 ± 0.36**
0.4%	6.03 ± 0.28	3.42 ± 0.49	5.12 ± 0.53	7.46 ± 0.28	6.2 ± 0.41	6 ± 0.44	6.9 ± 0.42	7.4 ± 0.46	**7.51 ± 0.59**
0.6%	6.8 ± 0.27	4.07 ± 0.41	6.8 ± 0.18	9.12 ± 0.27	8.7 ± 0.4	8.4 ± 0.42	8.2 ± 0.38	8.6 ± 0.43	**8.91 ± 0.41**
0.8%	7.96 ± 0.79	5.14 ± 0.7	8.42 ± 0.38	10.19 ± 0.79	9.8 ± 0.48	10.2 ± 0.49	10.5 ± 0.55	10.5 ± 0.5	**10.56 ± 0.24**
1%	9.38 ± 0.41	5.32 ± 0.33	11.53 ± 0.44	13.73 ± 0.41	13.2 ± 0.46	12.7 ± 0.45	12.1 ± 0.49	13.1 ± 0.47	**13.04 ± 0.54**
2%	12.74 ± 0.28	8.29 ± 0.45	15.9 ± 0.21	16.45 ± 0.28	17 ± 0.43	16.3 ± 0.43	16.4 ± 0.46	17.5 ± 0.45	**17.05 ± 0.22**
3%	16.58 ± 0.95	9.23 ± 0.52	18.24 ± 0.32	20.05 ± 0.95	21.1 ± 0.5	20 ± 0.46	20.3 ± 0.52	21.3 ± 0.49	**21.85 ± 0.85**
4%	19.99 ± 1.04	11.52 ± 1.16	23.82 ± 0.86	22.97 ± 1.04	24.5 ± 0.47	23.2 ± 0.44	23.9 ± 0.5	24.1 ± 0.46	**24.01 ± 0.24**
5%	22.41 ± 0.54	13.66 ± 1.35	26.38 ± 0.85	24.37 ± 0.54	27.8 ± 0.44	26.1 ± 0.41	27.1 ± 0.44	28.4 ± 0.43	**27.26 ± 0.83**
6%	23.66 ± 0.49	15.49 ± 0.92	28.16 ± 0.62	26.93 ± 0.49	29.9 ± 0.4	28.4 ± 0.39	29.4 ± 0.4	30.8 ± 0.4	**31.24 ± 0.19**
7%	28.36 ± 0.85	18.52 ± 0.56	30.95 ± 0.66	27.37 ± 0.85	32 ± 0.38	30.3 ± 0.36	31.5 ± 0.38	31.7 ± 0.37	**32.37 ± 0.71**
8%	30.75 ± 1.12	18.52 ± 0.39	31.84 ± 0.23	28.32 ± 1.12	33.2 ± 0.36	31.6 ± 0.34	32.6 ± 0.36	32.9 ± 0.35	**33.31 ± 0.68**
9%	32.12 ± 1.48	18.52 ± 0.98	32.79 ± 0.94	29.19 ± 1.48	34.4 ± 0.34	33 ± 0.33	33.8 ± 0.35	34.1 ± 0.34	**34.04 ± 0.74**
10%	32.75 ± 1.02	19.54 ± 0.85	33.04 ± 0.65	31.02 ± 1.02	35.8 ± 0.32	34.2 ± 0.31	35 ± 0.33	35.4 ± 0.32	**35.81 ± 0.21**
20%	35.63 ± 0.99	35.14 ± 1.06	37.12 ± 0.85	35.24 ± 0.81	39.6 ± 0.28	38.7 ± 0.27	40.1 ± 0.29	41.2 ± 0.28	**39.15 ± 0.57**
50%	43.17 ± 1.02	44.14 ± 0.4	45.78 ± 0.41	42.18 ± 0.69	47.2 ± 0.24	46 ± 0.23	48.3 ± 0.25	49 ± 0.24	**46.18 ± 0.13**
75%	63.21 ± 0.5	66.12 ± 0.46	66.12 ± 0.61	63.05 ± 0.41	65.8 ± 0.2	65.1 ± 0.19	66.9 ± 0.21	67.8 ± 0.2	**68.01 ± 0.82**

Table 3: Performance (top-1 accuracy) of optimization and training property-based coreset methods on CIFAR100 trainsplit. The coresets were selected and finetuned on ResNet-18. The full trainset performance was **70.95 ± 0.68**. The mean accuracy over 5 runs, along with their standard deviation, is reported.

Coreset Sizes	Random	CRAIG	Glister	GraphCut	SloCurv	TDDS	Dyn − Unc	DUAL	**CLD (Ours)**
0.2%	3.66 ± 0.41	3.5 ± 0.42	3.43 ± 0.32	5.8 ± 0.24	3.62 ± 0.44	3.7 ± 0.44	2.1 ± 0.55	2 ± 0.56	**5.67 ± 0.36**
0.4%	6.03 ± 0.28	5.8 ± 0.4	4.91 ± 0.37	7.07 ± 0.39	5.46 ± 0.36	6 ± 0.41	3.5 ± 0.5	3.4 ± 0.52	**7.51 ± 0.59**
0.6%	6.8 ± 0.27	7.9 ± 0.39	7.49 ± 0.61	8.96 ± 0.31	7.44 ± 0.2	8.2 ± 0.4	5.1 ± 0.48	5 ± 0.49	**8.91 ± 0.41**
0.8%	7.96 ± 0.79	9.8 ± 0.47	8.65 ± 0.47	9.39 ± 0.81	9.96 ± 0.42	10.1 ± 0.48	7 ± 0.53	7.2 ± 0.54	**10.56 ± 0.24**
1%	9.38 ± 0.41	12.2 ± 0.44	9.04 ± 0.43	11.86 ± 0.47	12.17 ± 0.3	12.8 ± 0.45	9.5 ± 0.5	10.4 ± 0.51	**13.04 ± 0.54**
2%	12.74 ± 0.28	15.9 ± 0.42	14.54 ± 0.41	16.95 ± 0.55	13.35 ± 0.42	16.5 ± 0.43	14.2 ± 0.47	15.8 ± 0.48	**17.05 ± 0.22**
3%	16.58 ± 0.95	19.6 ± 0.46	17.47 ± 0.32	19.21 ± 0.57	22.67 ± 0.8	20.3 ± 0.47	18.9 ± 0.5	20.5 ± 0.5	**21.85 ± 0.85**
4%	19.99 ± 1.04	23 ± 0.44	23.99 ± 0.58	21.33 ± 0.71	21.97 ± 0.55	23.7 ± 0.45	22.7 ± 0.48	24.3 ± 0.47	**24.01 ± 0.24**
5%	22.41 ± 0.54	25.8 ± 0.4	24.83 ± 0.73	26.31 ± 0.58	23.44 ± 0.71	26.6 ± 0.42	25.8 ± 0.44	27.5 ± 0.43	**27.26 ± 0.83**
6%	23.66 ± 0.49	28.1 ± 0.38	26.57 ± 0.69	30.35 ± 0.68	25.41 ± 0.43	28.9 ± 0.39	28.2 ± 0.41	30 ± 0.4	**31.24 ± 0.19**
7%	28.36 ± 0.85	30 ± 0.36	27.57 ± 0.84	31.63 ± 0.71	27.45 ± 0.6	30.8 ± 0.37	30.3 ± 0.38	32.1 ± 0.38	**32.37 ± 0.71**
8%	30.75 ± 1.12	31.3 ± 0.34	28.79 ± 0.8	32.22 ± 0.48	29.17 ± 0.47	32 ± 0.35	31.7 ± 0.36	33.4 ± 0.35	**33.31 ± 0.68**
9%	32.12 ± 1.48	32.7 ± 0.32	30.22 ± 0.32	33.02 ± 0.83	30.71 ± 0.57	33.4 ± 0.33	33 ± 0.34	34.8 ± 0.33	**34.04 ± 0.74**
10%	32.75 ± 1.02	34.1 ± 0.3	31.22 ± 1.33	34.41 ± 0.96	33.17 ± 1.16	34.7 ± 0.31	34.4 ± 0.32	36.2 ± 0.31	**35.81 ± 0.21**
20%	35.63 ± 0.99	38.2 ± 0.26	36.49 ± 0.47	38.02 ± 0.52	37.23 ± 0.81	39.1 ± 0.27	38.8 ± 0.28	40.5 ± 0.27	**39.15 ± 0.57**
50%	43.17 ± 1.02	45.6 ± 0.22	41.81 ± 0.88	45.23 ± 0.42	45.19 ± 0.42	46.5 ± 0.23	45.8 ± 0.24	47.5 ± 0.23	**46.18 ± 0.13**
75%	63.21 ± 0.5	64.8 ± 0.19	63.85 ± 1.02	65.18 ± 0.32	66.53 ± 0.61	65.9 ± 0.2	64.5 ± 0.2	66.2 ± 0.19	**68.01 ± 0.82**

Table 4: Performance (top-1 accuracy) of score-based coreset methods on ImageNet-1k trainsplit. The coresets were selected and finetuned on ResNet-18. The full trainset performance was $\mathbf{69.91 \pm 0.01}$. The mean accuracy over 5 runs, along with their standard deviation, is reported.

Coreset Sizes	Random	Herding	Forgetting	Cal	EL2N	Moderate	CCS(AUM)	$\mathbb{D}^2$-Pruning	**CLD**
0.1%	0.7 ± 0.03	0.31 ± 0.01	0.64 ± 0.01	1.13 ± 0.12	0.88 ± 0.25	0.85 ± 0.2	1.52 ± 0.5	1.95 ± 0.4	**1.96** $\pm$ **0.7**
0.5%	3.98 ± 0.19	1.39 ± 0.17	4.78 ± 1.01	6.84 ± 0.13	5.83 ± 0.1	4.75 ± 0.5	7.04 ± 0.1	7.2 ± 0.25	**7.16** $\pm$ **0.63**
1%	7.86 ± 0.43	4.32 ± 0.62	12.67 ± 0.51	13.17 ± 0.22	15.2 ± 0.5	14.32 ± 1.03	14.86 ± 0.25	16.01 ± 0.4	**15.92** $\pm$ **0.41**
5%	39.78 ± 0.23	15.36 ± 0.18	44.86 ± 0.74	37.65 ± 1.3	40.43 ± 0.03	38.95 ± 0.25	44.04 ± 0.1	45.75 ± 0.5	**46.5** $\pm$ **0.19**
10%	51.24 ± 0.04	26.84 ± 0.05	53.19 ± 0.06	44.16 ± 0.78	45.16 ± 0.4	44.56 ± 0.1	52.01 ± 0.2	50.65 ± 0.3	**53.81** $\pm$ **0.23**
30%	60.87 ± 0.13	46.61 ± 0.87	60.9 ± 0.05	54.41 ± 0.45	53.22 ± 0.25	55.29 ± 0.1	61.84 ± 0.5	60.75 ± 0.1	**62.91** $\pm$ **0.51**
40%	62.13 ± 0.38	53.88 ± 0.23	62.39 ± 0.91	58.45 ± 0.92	56.45 ± 0.1	60.08 ± 0.15	62.48 ± 0.02	61.04 ± 0.5	**63.51** $\pm$ **0.75**
50%	64.11 ± 0.12	59.14 ± 0.41	63.18 ± 0.05	60.11 ± 0.6	59.46 ± 0.45	62.58 ± 0.25	64.31 ± 0.04	64.92 ± 0.65	**65.78** $\pm$ **1.03**
65%	65.21 ± 0.03	64.23 ± 0.2	65.24 ± 0.02	64.42 ± 0.01	61.28 ± 0.25	64.98 ± 0.1	65.17 ± 0.1	67.01 ± 0.1	**68.02** $\pm$ **0.38**
70%	68.81 ± 0.04	65.22 ± 0.02	67.85 ± 0.9	66.57 ± 0.03	64.23 ± 0.89	65.18 ± 0.03	68.81 ± 0.1	68.91 ± 0.01	**68.91** $\pm$ **0.01**
75%	68.41 ± 0.02	67.42 ± 0.01	68.01 ± 0.1	67.12 ± 0.02	65.45 ± 0.2	67.13 ± 0.03	69.01 ± 0.03	69.42 ± 0.05	**69.42** $\pm$ **0.05**
80%	68.12 ± 0.03	68.02 ± 0.02	68.81 ± 0.5	68.15 ± 0.03	66.95 ± 0.25	68.9 ± 0.01	69.93 ± 0.02	69.93 ± 0.02	**69.93** $\pm$ **0.02**
85%	68.75 ± 0.05	68.01 ± 0.03	68.81 ± 0.5	68.91 ± 0.04	67.17 ± 0.1	68.9 ± 0.2	69.91 ± 0.25	69.93 ± 0.02	**69.93** $\pm$ **0.02**
90%	69.1 ± 0.78	69.92 ± 0.4	70.04 ± 0.52	69.23 ± 0.5	68.81 ± 0.3	69.01 ± 0.2	70.12 ± 0.03	70.12 ± 0.03	**70.12** $\pm$ **0.03**
95%	69.91 ± 0.06	69.91 ± 0.04	69.91 ± 0.04	70.12 ± 0.01	69.91 ± 0.04	70.12 ± 0.03	69.91 ± 0.1	70.12 ± 0.03	**70.12** $\pm$ **0.03**

Table 5: Performance (top-1 accuracy) of optimization and training property-based coreset methods on ImageNet-1k trainsplit. The coresets were selected and finetuned on ResNet-18. The full trainset performance was **69.91 ± 0.01**. The mean accuracy over 5 runs, along with their standard deviation, is reported.

Coreset Sizes	Random	CRAIG	Glister	GraphCut	SloCurv	TDDS	Dyn − Unc	DUAL	**CLD**
0.1%	0.7 ± 0.03	0.94 ± 0.1	0.86 ± 0.01	1.09 ± 0.09	1.23 ± 0.06	1.04 ± 0.2	0.45 ± 0.9	0.41 ± 1.06	**1.96 ± 0.7**
0.5%	3.98 ± 0.19	6.41 ± 0.25	5.55 ± 0.05	7.27 ± 0.03	5.89 ± 0.07	5.64 ± 0.03	1.45 ± 1.05	1.34 ± 0.87	**7.16 ± 0.63**
1%	7.86 ± 0.43	15.56 ± 0.05	12.45 ± 0.01	14.27 ± 0.31	14.17 ± 0.02	14.05 ± 0.1	3.92 ± 0.8	4.85 ± 0.75	**15.92 ± 0.41**
5%	39.78 ± 0.23	39.95 ± 0.01	42.19 ± 0.03	39.8 ± 0.6	40.1 ± 0.14	40.54 ± 0.05	15.98 ± 0.5	16.2 ± 0.4	**46.5 ± 0.19**
10%	51.24 ± 0.04	46.76 ± 0.1	50.1 ± 0.01	48.27 ± 1.02	46.39 ± 0.5	46.45 ± 0.25	29.78 ± 0.6	50.75 ± 0.5	**53.81 ± 0.23**
30%	60.87 ± 0.13	55.41 ± 0.05	58.53 ± 0.05	61.23 ± 0.01	57.19 ± 0.01	57.24 ± 0.1	50.16 ± 0.5	60.19 ± 0.03	**62.91 ± 0.51**
40%	62.13 ± 0.38	56.55 ± 0.02	61.72 ± 0.02	63.23 ± 0.08	62.11 ± 0.67	62.23 ± 0.5	60.25 ± 0.2	63.45 ± 0.25	**63.51 ± 0.75**
50%	64.11 ± 0.12	58.56 ± 0.5	63.41 ± 0.51	65.17 ± 0.05	64.78 ± 0.13	63.96 ± 0.81	63.17 ± 0.1	65.21 ± 0.04	**65.78 ± 1.03**
65%	65.21 ± 0.03	63.41 ± 0.2	65.83 ± 0.02	67.91 ± 0.54	65.81 ± 0.02	65.19 ± 0.1	65.98 ± 0.25	68.31 ± 0.01	**68.02 ± 0.38**
70%	68.81 ± 0.04	65.21 ± 0.01	67.91 ± 0.03	68.52 ± 0.04	67.18 ± 0.03	67.25 ± 0.01	66.32 ± 0.1	68.76 ± 0.5	**68.91 ± 0.01**
75%	68.41 ± 0.02	68.01 ± 0.5	68.54 ± 0.46	68.81 ± 0.02	68.03 ± 0.15	68.14 ± 0.25	68.19 ± 0.01	69.92 ± 0.01	**69.42 ± 0.05**
80%	68.12 ± 0.03	68.01 ± 0.5	68.78 ± 0.02	69.12 ± 0.05	69.1 ± 0.14	68.91 ± 0.2	68.19 ± 0.01	69.92 ± 0.01	**69.93 ± 0.02**
85%	68.75 ± 0.05	68.78 ± 0.02	68.78 ± 0.02	70.01 ± 0.28	69.1 ± 0.02	68.91 ± 0.25	69.93 ± 0.2	69.93 ± 0.2	**69.93 ± 0.02**
90%	69.1 ± 0.78	68.48 ± 0.25	69.18 ± 0.34	70.12 ± 0.43	69.68 ± 0.03	69.68 ± 0.03	70.12 ± 0.03	70.12 ± 0.03	**70.12 ± 0.03**
95%	69.91 ± 0.06	69.91 ± 0.04	69.91 ± 0.04	70.12 ± 0.43	69.91 ± 0.04	69.68 ± 0.03	70.12 ± 0.03	70.12 ± 0.03	**70.12 ± 0.03**

Table 6: Cross-architecture performance of coresets of different sizes of ImageNet-1k identified by `CLD`. Each cell reports mean test accuracy (top) and standard deviation (bottom) over 5 runs. Minimal accuracy drop (< 1%) is observed when transferring coresets from a smaller ResNet-18 model to larger or different architectures.

Target Model	Source Model	Coreset size (% of dataset)							
		5%	10%	25%	40%	50%	75%	80%	100%
ResNet-34	ResNet-18	46.91 ± 0.03	54.83 ± 0.05	60.21 ± 0.12	66.83 ± 0.48	68.93 ± 0.01	71.12 ± 0.01	73.04 ± 0.05	73.21 ± 0.01
ResNet-34	ResNet-34	47.01 ± 0.02	54.75 ± 0.35	60.98 ± 0.71	67.26 ± 0.10	69.03 ± 0.04	71.06 ± 0.02	73.04 ± 0.01	73.21 ± 0.01
ResNet-50	ResNet-18	47.19 ± 0.01	56.14 ± 0.05	62.83 ± 0.13	68.14 ± 0.01	71.15 ± 0.03	73.04 ± 0.07	74.95 ± 0.02	75.81 ± 0.05
ResNet-50	ResNet-50	48.10 ± 0.05	57.03 ± 0.03	63.14 ± 0.02	68.91 ± 0.05	71.25 ± 0.04	73.57 ± 0.01	74.95 ± 0.02	75.81 ± 0.05
DenseNet-121	ResNet-18	45.18 ± 0.37	55.18 ± 0.61	61.19 ± 0.01	67.34 ± 0.04	71.02 ± 0.83	71.85 ± 0.04	73.85 ± 0.02	74.90 ± 0.37
DenseNet-121	DenseNet-121	46.07 ± 0.02	55.88 ± 0.03	62.01 ± 0.72	67.91 ± 0.61	71.36 ± 0.10	72.18 ± 0.07	74.04 ± 0.04	74.90 ± 0.37
VGG-19(bn)	ResNet-18	43.12 ± 0.04	53.18 ± 0.03	60.12 ± 0.02	66.17 ± 0.07	70.37 ± 0.01	72.01 ± 0.04	73.98 ± 0.37	74.70 ± 0.71
VGG-19(bn)	VGG-19(bn)	44.01 ± 0.50	54.12 ± 0.47	61.01 ± 0.31	67.09 ± 0.16	70.25 ± 0.25	72.58 ± 0.02	74.05 ± 0.04	74.70 ± 0.71

D Additional Ablations

D.1 Stability across random seeds

We measure sensitivity to random initialization by computing per-example `CLD` scores across five independent seeds on ImageNet-1k (ResNet-18). The pairwise mean absolute error (MAE) between score vectors is consistently below 10^{-5}, indicating negligible variance and high reproducibility; see Figure 7a.

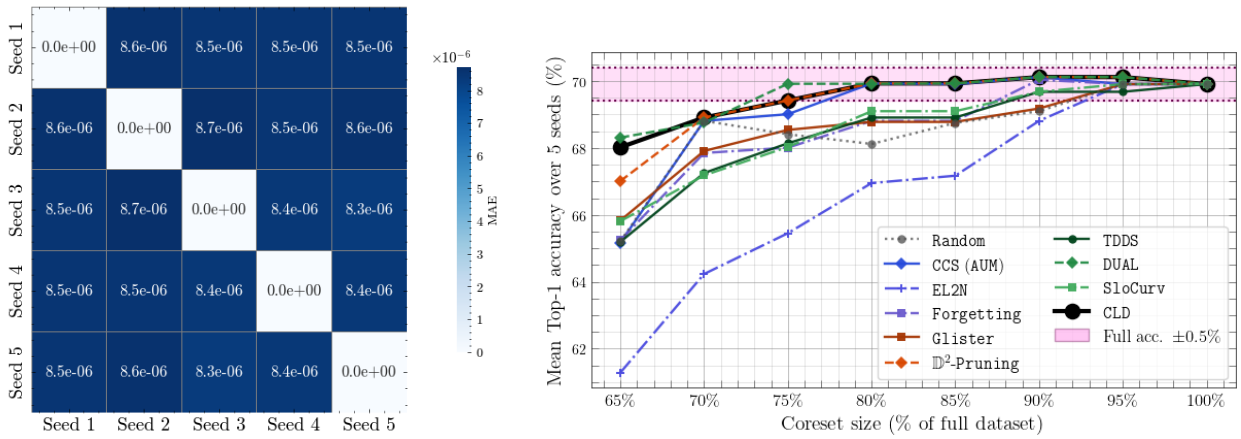

(a) **Seed reproducibility.** Pairwise MAE of `CLD` scores across 5 seeds (lower is better).

(b) **Subset size vs. accuracy.** ImageNet-1k, ResNet-18. The shaded band marks the 0.5% tolerance below full-data accuracy.

Figure 7: Seed-wise stability and subset-size trade-offs on ImageNet-1k.

D.2 Minimum subset size for full-data accuracy

We quantify the subset fraction required to recover near full-data performance on ImageNet-1k (ResNet-18). As shown in Figure 7b, `CLD` attains test accuracy within 0.5% of the full-data model using only 75% of the training set, on par with $\mathbb{D}^2$-`Pruning` and `DUAL`, and superior to other baselines we evaluated.

E Detailed Explanation of Compute and Storage Cost of Coreset Methodologies

Recap of Notation We denote the number of training samples by N ($\mathbf{S} \sim \mathbf{D}^N$) and the number of query (held-out validation) samples by Q ($\mathbf{V} \sim \mathbf{D}^Q$). The model is trained for T epochs. Certain TDA metrics have hyperparameters (denoted λ_τ) used to compute the TDA metric τ, which may influence computational cost.

We measure computation in floating-point operations (FLOPs). Let f_{large} be the cost of a *single-example* forward pass for the large model with p_{large} parameters, and approximate the backward-pass cost as $2f_{\text{large}}$. When a proxy (smaller) model is used, we write its per-example forward cost and parameter count as f and p, with $f \ll f_{\text{large}}$ and $p \ll p_{\text{large}}$.

R is the number of model retrainings (when applicable). k is the coreset size; d is the feature dimensionality; and B is the minibatch size (used during training but not appearing in per-example FLOP counts). Some methods perform subset *reselection* during training; when used, we denote the reselection interval (in epochs) by γ.

Reference: full-data training (large model) Training the large model on all N points for T epochs costs $3NT\, f_{\text{large}}$ FLOPs and stores p_{large} parameters (ignoring optimizer state). Totals below are the end-to-end cost to (i) select a coreset of size k and (ii) train the large model on that coreset.

Example scenario (used for all plug-in estimates). To further illustrate the computational efficiency of `CLD`, we provide approximate cost values by substituting the values of the parameters for finding and training a 10% coreset on the ImageNet-1k dataset.

- N=1,268,355 (99% of train), Q=12,812 (remaining 1%), d=224×224×3, c=1000.
- Size of coreset k=126,836.
- Proxy encoder: ResNet-18 with p=11,689,128 and per-example forward FLOPs f=1,818,228,160.
- Large model: ResNet-50 with p_{large}=25,557,032 and f_{large}≈8,178,000,000.
- We use the standard ImageNet recipe of T=T_{proxy}=90 epochs (Yang, 2017).
- When a method has additional parameters, we use the paper's choice (e.g., in `Glister`, γ=20).

E.1 Score-based Methods

E.1.1 Kernel Herding (`Herding`)

`Herding` (Chen et al., 2010) iteratively constructs a representative subset by approximating the data distribution in an RKHS. At iteration t, it selects

$$\vec{z}^{*t} \;=\; \arg\max_{\vec{z}\in\mathbf{S}} \langle w_{t-1},\, \phi(\vec{z})\rangle,$$

where $\phi(\cdot)$ is the kernel feature map and w_{t-1} is an RKHS weight vector. Repeating for k iterations yields a size-k coreset.

Execution. One-time selection prior to training the large model (a proxy encoder is used to obtain features):

i) *Train proxy encoder:* train a proxy model for T_{proxy} epochs (forward cost f, parameters p).
ii) *Encode full dataset:* extract features for all N points using the trained proxy (Nf FLOPs).
iii) *Herding selection:* for t=1:k, update candidate scores and select $\vec{z}^{*t}$ using inner products in feature space (explicit features of dim. d give $\mathcal{O}(Nd)$ per iteration, i.e., $\mathcal{O}(Ndk)$ total).
iv) *Train on coreset:* train the large model on the selected k points for T_{late} epochs (here T_{late}=T).

End-to-end compute (selection + coreset training).

$$\boxed{\text{Compute}_{\texttt{Herding}} = \underbrace{3N\,T_{\text{proxy}}\,f}_{\text{train proxy}} + \underbrace{Nf}_{\text{feature extraction}} + \underbrace{\mathcal{O}(Ndk)}_{\text{iterative herding updates}} + \underbrace{3k\,T_{\text{late}}\,f_{\text{large}}}_{\text{train large on coreset}}}$$

Selection-stage storage overhead. Storing explicit features dominates; caching a $k \times k$ Gram among selected points is optional:

$$\boxed{\text{StorageOverhead}_{\texttt{Herding}} = \mathcal{O}(Nd) \quad (+\,\mathcal{O}(k^2) \text{ optional Gram})}$$

Example scenario values (ImageNet-1k; T_{late}=90, T_{proxy}=90).

$$\text{Compute}_{\texttt{Herding}}\ (\text{PFLOPs only}) \approx \underbrace{622.663}_{3NT_{\text{proxy}}f} + \underbrace{2.306}_{Nf} + \underbrace{280.061}_{3kT_{\text{late}}\,f_{\text{large}}} = \mathbf{905.031}\ \text{PFLOPs},$$

(negligible herding updates)

$$\text{StorageOverhead}_{\texttt{Herding}}(\text{float32}) \approx Nd \times 4 = \mathbf{763.692}\ \text{GB (features only)}.$$

E.1.2 Example Forgetting (`Forgetting`)

`Forgetting` (Toneva et al., 2018) measures, for each training sample, how many times it transitions from being correctly classified to incorrectly classified during training ("forgetting events"). Examples with higher forgetting counts are ranked as more informative.

Execution. One-time selection prior to training the large model on the coreset. Let T_{early} be the number of early epochs run on the full dataset to collect forgetting statistics, and $T_{\text{late}} = T - T_{\text{early}}$ the remaining epochs used to train on the selected coreset:

i) Train on all N points for T_{early} epochs while tracking, per example, the previous correctness bit and a forgetting counter (constant-time update per visit).
ii) Select the top k examples by forgetting count; train the large model on this coreset for T_{late} epochs.

End-to-end compute (selection + coreset training).

$$\boxed{\text{Compute}_{\texttt{Forgetting}} = \underbrace{3N\,T_{\text{early}}\,f_{\text{large}}}_{\text{collect forgetting on full data}} + \underbrace{3k\,T_{\text{late}}\,f_{\text{large}}}_{\text{train large on coreset}}}$$

Selection-stage storage overhead. Streaming the metric requires only one scalar counter (and one correctness bit) per training example:

$$\boxed{\text{StorageOverhead}_{\texttt{Forgetting}} = \mathcal{O}(N) \quad (\text{per-sample counter/bit})}$$

Example scenario values (ImageNet-1k; T_{early}=10, T_{late}=80).

$$\text{Compute}_{\texttt{Forgetting}}\ (\text{PFLOPs only}) \approx \underbrace{311.178}_{3NT_{\text{early}}\,f_{\text{large}}} + \underbrace{248.943}_{3kT_{\text{late}}\,f_{\text{large}}} = \mathbf{560.122}\ \text{PFLOPs},$$

$$\text{StorageOverhead}_{\texttt{Forgetting}}(\text{float32}) \approx N \times 4 = 5{,}073{,}420\ \text{B} = \mathbf{0.005}\ \text{GB}.$$

E.1.3 Area Under Margin (`AUM`)

`AUM` (Pleiss et al., 2020) scores each training sample by aggregating its *margin* over training (e.g., logit of the true class minus the max non-true logit), producing the *area under the margin* across epochs/updates. Higher absolute AUM indicates more consistently confident predictions; lower AUM can flag ambiguous or noisy samples. We compute AUM with a *proxy* model and then train the large model on the selected coreset.

Execution. One-time selection with a proxy; the large model then trains on the coreset for all T epochs:

i) *Train proxy & log margins:* train a proxy for T_{proxy} epochs on all N samples (per-example forward cost f, parameters p), recording each sample's margin as it appears in training (no extra forward/backward beyond training).
ii) *Compute AUM & select:* for each sample, aggregate (e.g., sum/average) its logged margins to obtain AUM and select a size-k coreset according to the desired criterion (e.g., highest AUM, or filter low-AUM points).
iii) *Train large on coreset:* train the large model on the selected k samples for T epochs.

End-to-end compute (selection + coreset training).

$$\boxed{\text{Compute}_{\texttt{AUM}} = \underbrace{3N\,T_{\text{proxy}}\,f}_{\text{train proxy (margin logging piggybacks)}} + \underbrace{3k\,T\,f_{\text{large}}}_{\text{train large on coreset}}}$$

Selection-stage storage overhead. AUM can be streamed with a running sum/count per sample:

$$\boxed{\text{StorageOverhead}_{\texttt{AUM}} = \mathcal{O}(N) \quad \text{(running sums)}}$$

Example scenario values (ImageNet-1k; T_{proxy}=90, T=90).

$$\text{Compute}_{\texttt{AUM}}\ (\text{PFLOPs only}) \approx \underbrace{622.663}_{3NT_{\text{proxy}}f} + \underbrace{280.061}_{3kT\,f_{\text{large}}} = \mathbf{902.724}\ \text{PFLOPs},$$

$$\text{StorageOverhead}_{\texttt{AUM}}\ (\text{float32}) \approx N \times 4 = 5{,}073{,}420\ \text{B} = \mathbf{0.005}\ \text{GB}.$$

E.1.4 Contrastive Active Learning (`Cal`)

`Cal` (Margatina et al., 2021) acquires unlabeled examples that are near labeled ones in feature space yet differ in predictive probabilities (contrastive pairs), using nearest neighbors over encoder features and a simple divergence-based ranking.

Execution. A one-time selection stage is performed prior to training the large model:

i) train a *proxy* model from scratch on the (growing) labeled set up to size k (per-example forward cost $f \ll f_{\text{large}}$);
ii) encode all U unlabeled points with the trained proxy (here U=N);
iii) run kNN-style neighbor search between the unlabeled pool and the labeled set (size k), and select a coreset of size k.

(The divergence computation is much cheaper than (ii)–(iii) and is absorbed into big-$\mathcal{O}$.)

Overall compute (select once, then train-on-coreset).

$$\boxed{\text{Compute}_{\texttt{Cal}} = \underbrace{3k\,T_{\text{proxy}}\,f}_{\text{train proxy}} + \underbrace{U\,f}_{\text{encode unlabeled pool}} + \underbrace{\mathcal{O}(U\,k\,d)}_{k\text{NN over features}} + \underbrace{3kT\,f_{\text{large}}}_{\text{train large on coreset}}}$$

Selection-stage storage overhead. Storage overhead is due to the cached features for the unlabeled pool

$$\boxed{\text{StorageOverhead}_{\texttt{Cal}} = \mathcal{O}(Ud) \quad \text{(proxy features)}}$$

Example scenario values: ImageNet-1k; U=N).

$$\text{Compute}_{\texttt{Cal}}\ (\text{PFLOPs only}) \approx \underbrace{62.267}_{3kT_{\text{proxy}}f} + \underbrace{2.306}_{Uf\ (U=N)} + \underbrace{280.061}_{3kT\,f_{\text{large}}} = \mathbf{344.634}\ \text{PFLOPs},$$

$$\text{StorageOverhead}_{\texttt{Cal}}\ (\text{float32}) \approx Ud \times 4 = \mathbf{763.739}\ \text{GB}.$$

E.1.5 Gradient and Error L2 Norm-based Data Pruning (`GraNd`, `EL2N`)

`GraNd` (Paul et al., 2021) ranks training examples by the (expected) per-example gradient norm early in training:

$$\mathrm{GraNd}_t(\vec{z}_m) = \mathbb{E}_{\theta_t} \left\| \nabla_{\theta_t} \ell(\theta_t, \vec{z}_m) \right\|_2^2,$$

averaged over multiple random initializations and early epochs, then retains the top-k examples.

`EL2N` (Paul et al., 2021) ranks examples by the (expected) L2 error of predictions early in training:

$$\mathrm{EL2N}_t(\vec{z}_m) = \mathbb{E}_{\theta_t} \left\| \mathbf{p}_\theta(\vec{x}_m) - \mathbf{y}_m \right\|_2,$$

where $\mathbf{p}_\theta$ are class probabilities and $\mathbf{y}_m$ is the one-hot label. Scores are computed at small t and optionally averaged over R runs.

Execution. One-time selection prior to training the large model. Let T_{early} be the number of early epochs used for scoring and $T_{\text{late}} = T - T_{\text{early}}$ the remaining epochs used to train on the coreset:

i) For each of R initializations, train on all N points for T_{early} epochs (costing $3NT_{\text{early}} f_{\text{large}}$) while logging per-example predictions.
   (a) `EL2N`: compute scores directly from the logged predictions (no extra passes).
   (b) `GraNd`: run an *additional scoring sweep* to obtain per-sample gradients (one forward + one backward pass per example per early epoch).

ii) Average scores across runs; keep the top k; train the large model on the coreset for T_{late} epochs.

End-to-end compute (selection + train-on-coreset).

$$\boxed{\begin{aligned} \mathrm{Compute}_{\texttt{EL2N}} &= \underbrace{3N\,T_{\text{early}}\,R\,f_{\text{large}}}_{\text{early training (errors reused)}} + \underbrace{3k\,T_{\text{late}}\,f_{\text{large}}}_{\text{train large on coreset}}, \\ \mathrm{Compute}_{\texttt{GraNd}} &= \underbrace{3N\,T_{\text{early}}\,R\,f_{\text{large}}}_{\text{early training}} + \underbrace{3N\,T_{\text{early}}\,R\,f_{\text{large}}}_{\text{extra per-sample gradient sweeps}} + \underbrace{3k\,T_{\text{late}}\,f_{\text{large}}}_{\text{train large on coreset}}. \end{aligned}}$$

Selection-stage storage overhead. During scoring, a running vector of N scalar scores need to be stored:

$$\boxed{\begin{aligned} \mathrm{StorageOverhead}_{\texttt{EL2N}} &= \mathcal{O}(N), \\ \mathrm{StorageOverhead}_{\texttt{GraNd}} &= \mathcal{O}(N). \end{aligned}}$$

Example scenario values (ImageNet-1k; R=10, T_{early}=10, T_{late}=80).

$$\mathrm{Compute}_{\texttt{EL2N}}\ (\text{PFLOPs only}) \approx \underbrace{3{,}111.782}_{3NT_{\text{early}}R\,f_{\text{large}}} + \underbrace{248.943}_{3kT_{\text{late}}\,f_{\text{large}}} = \mathbf{3{,}360.725}\ \text{PFLOPs},$$

$$\mathrm{Compute}_{\texttt{GraNd}}\ (\text{PFLOPs only}) \approx \underbrace{3{,}111.782}_{\text{early training}} + \underbrace{3{,}111.782}_{\text{extra gradient sweeps}} + \underbrace{248.943}_{3kT_{\text{late}}\,f_{\text{large}}} = \mathbf{6{,}472.507}\ \text{PFLOPs},$$

$$\mathrm{StorageOverhead}\ (\text{float32}) \approx N \times 4 = \mathbf{0.005}\ \text{GB for each.}$$

E.1.6 Using Class Feature Medians (`Moderate`)

`Moderate` (Xia et al., 2022) builds a representative coreset by selecting, *within each class*, the samples whose feature-to-center distances are closest to that class's *median* distance (thus avoiding both easy near-center redundancies and far-out outliers). We compute class centers and distances in a proxy feature space.

Execution. One-time selection with a proxy, then train the large model on the coreset for all T epochs:

i) *Train proxy:* train a proxy encoder on all N samples for T_{proxy} epochs (per-example forward cost f, parameters p).
ii) *Encode dataset:* extract proxy features for all N samples (cost Nf FLOPs).
iii) *Class-median selection:* for each class, compute the class center and all sample distances, then select the per-class quota of samples whose distances are closest to the class-wise median (distance computation $\mathcal{O}(Nd)$; median/quantile selection $\mathcal{O}(N \log N)$ or linear-time selection).
iv) *Train large on coreset:* train the large model on the selected k samples for T epochs.

End-to-end compute (selection + coreset training).

$$\boxed{\text{Compute}_{\texttt{Moderate}} = \underbrace{3N\,T_{\text{proxy}}\,f}_{\text{train proxy}} + \underbrace{Nf}_{\text{feature extraction}} + \underbrace{\mathcal{O}\big(Nd + N\log N\big)}_{\text{class centers, distances, medians}} + \underbrace{3k\,T\,f_{\text{large}}}_{\text{train large on coreset}}}$$

Selection-stage storage overhead. The main storage overhead is from caching the features during selection

$$\boxed{\text{StorageOverhead}_{\texttt{Moderate}} = \mathcal{O}(Nd) \;\; \text{(proxy features)}}$$

Example scenario values (ImageNet-1k; T_{proxy}=90, T=90).

$$\text{Compute}_{\texttt{Moderate}}\ (\text{PFLOPs only}) \approx \underbrace{622.663}_{3NT_{\text{proxy}}f} + \underbrace{2.306}_{Nf} + \underbrace{280.061}_{3kT\,f_{\text{large}}} = \mathbf{905.031}\ \text{PFLOPs},$$

$$\text{StorageOverhead}_{\texttt{Moderate}}(\text{float32}) \approx Nd \times 4 = \mathbf{763.739}\ \text{GB}.$$

E.1.7 Message Passing ($\mathbb{D}^2 - \texttt{Pruning}$)

$\mathbb{D}^2\texttt{Pruning}$ (Maharana et al., 2024) selects a coreset by *balancing difficulty and diversity* via message passing on a dataset graph built from proxy features. Initial per-sample difficulty scores (from the proxy) are diffused over a kNN graph so that each example's score incorporates information from its neighbors; a graph-based sampler then selects a subset that covers diverse yet difficult regions.

Execution. One-time selection with a proxy, then train the large model on the coreset for all T epochs:

i) *Train proxy:* train a proxy encoder on all N samples for T_{proxy} epochs (per-example forward cost f, parameters p).
ii) *Encode dataset:* extract proxy features for all N samples (cost Nf FLOPs).
iii) *Build graph:* construct a kNN graph over the features (e.g., ANN); cost $\mathcal{O}(N\,k\,d)$ (or $\mathcal{O}(N\,d\log N)$).
iv) *Message passing & sampling:* run H rounds of (forward/reverse) message passing on the $N \times k$ edges to update difficulty-aware scores, then sample a size-k coreset (cost $\mathcal{O}(H\,N\,k)$ plus linear-time sampling).
v) *Train large on coreset:* train the large model on the selected k samples for T epochs.

End-to-end compute (selection + coreset training).

$$\boxed{\text{Compute}_{\mathbb{D}^2\texttt{Pruning}} = \underbrace{3N\,T_{\text{proxy}}\,f}_{\text{train proxy}} + \underbrace{Nf}_{\text{feature extraction}} + \underbrace{\mathcal{O}(N\,k\,d) + \mathcal{O}(H\,N\,k)}_{\text{graph build \& message passing}} + \underbrace{3k\,T\,f_{\text{large}}}_{\text{train large on coreset}}}$$

Selection-stage storage overhead. Caching proxy features dominates; the kNN adjacency is linear in N and smaller in practice:

$$\boxed{\text{StorageOverhead}_{\mathbb{D}^2\texttt{Pruning}} = \mathcal{O}(Nd) \;+\; \mathcal{O}(N\kappa) \;\; \text{(features + } k\text{NN graph)}}$$

Example scenario values (ImageNet-1k; T_{proxy}=90, T=90).

$$\text{Compute}_{\mathbb{D}^2\texttt{Pruning}}\ (\text{PFLOPs only}) \approx \underbrace{622.663}_{3NT_{\text{proxy}}f} + \underbrace{2.306}_{Nf} + \underbrace{280.061}_{3kT\,f_{\text{large}}} = \mathbf{905.031}\ \text{PFLOPs}, \quad \text{(excluding graph terms)}$$

$$\text{StorageOverhead}_{\mathbb{D}^2\texttt{Pruning}}\ (\text{float32}) \approx Nd \times 4 = \mathbf{763.692}\ \text{GB}.$$

E.2 Optimization-based Methods

E.2.1 Gradient Matching Optimization (CRAIG)

CRAIG (Mirzasoleiman et al., 2020) selects a subset whose (aggregated) gradients closely match those of the full dataset across training, typically using a submodular (stochastic-greedy) objective over *per-sample gradient embeddings* at selected *anchor* epochs. We compute embeddings with a proxy model and then train the large model on the coreset for all T epochs.

Execution. One-time selection with a proxy, then train the large model:

i) *Train proxy:* train a proxy network on all N samples for T_{proxy} epochs (per-example forward cost f, parameters p).
ii) *Per-sample gradient embeddings at anchors:* every γ_{anc} epochs (anchors $A{=}T_{\text{proxy}}/\gamma_{\text{anc}}$), compute for each sample the *last-layer* gradient embedding using only forward-pass outputs:

$$g_i^{(a)} \;=\; \big(\mathbf{p}_\theta^{(a)}(\vec{x}_i) - \mathbf{y}_i\big) \;\oplus\; h_\theta^{(a)}(\vec{x}_i),$$

where h_θ is the penultimate representation (dim. F) and $\mathbf{p}_\theta - \mathbf{y}_i \in \mathbb{R}^C$ is the class-probability error; this avoids backward passes (piggybacks on training). Selection then runs stochastic-greedy on these embeddings per anchor.
iii) *Select & train large:* union the anchor-wise selections to a size-k coreset and train the large model on it for all T epochs.

End-to-end compute (selection + coreset training).

$$\boxed{\text{Compute}_{\texttt{CRAIG}} = \underbrace{3N\,T_{\text{proxy}}\,f}_{\text{train proxy (embeddings piggyback)}} + \underbrace{\mathcal{O}\big(A\,(Nk + N\log(1/\epsilon))\,D_{\text{eff}}\big)}_{\text{stochastic-greedy over anchors}} + \underbrace{3k\,T\,f_{\text{large}}}_{\text{train large on coreset}}}$$

Here $D_{\text{eff}} \approx F{+}C$ is the embedding dimensionality (penultimate features and class-probability error); the submodular arithmetic is negligible in FLOPs relative to training and is kept in big-$\mathcal{O}$.

Selection-stage storage overhead. We stream anchor processing so only a single anchor's embeddings need be cached at once:

$$\boxed{\text{StorageOverhead}_{\texttt{CRAIG}} = \mathcal{O}\big(N(F{+}C)\big) \quad \text{(per-anchor embeddings, streamed per anchor)}}$$

Example scenario values (ImageNet-1k; T_{proxy}=90, T=90, F=512, C=1000).

$$\text{Compute}_{\texttt{CRAIG}} \text{ (PFLOPs only; excluding big-}\mathcal{O}\text{ selection)} \approx \underbrace{622.663}_{3NT_{\text{proxy}}f} + \underbrace{280.061}_{3kT\,f_{\text{large}}} = \mathbf{902.724} \text{ PFLOPs},$$

$$\text{Storage}_{\texttt{CRAIG}} \text{ (float32)} \approx N(F{+}C) \times 4 = \mathbf{7.671} \text{ GB}.$$

E.2.2 Generalization-based Data Subset Selection for Efficient and Robust Learning (Glister)

Glister (Killamsetty et al., 2021b) selects $\mathbf{S}_j$ of size k via a mixed discrete–continuous bi-level objective:

$$\underset{\mathbf{S}_j \subseteq \mathbf{S},\, |\mathbf{S}_j| \le k}{\arg\max} \; \mathcal{L}_{\mathbf{V}}\big(\theta^\star(\mathbf{S}_j)\big) \quad \text{where} \quad \theta^\star(\mathbf{S}_j) = \underset{\theta}{\arg\max}\; \mathcal{L}_{\mathbf{S}}(\theta; \mathbf{S}_j).$$

Execution. Glister *replaces the training loop*: it interleaves training on the current subset with periodic re-selection every γ epochs (using stochastic-greedy with a Taylor approximation).

Overall compute (train-on-coreset). Training on the coreset over T epochs costs $3kT\,f_{\text{large}}$. Selection across T epochs at frequency γ costs $\mathcal{O}\left(\frac{\big(kQ+N\log(1/\epsilon)\big)\,f_{\text{large}}\,T}{\gamma}\right)$. Hence

$$\boxed{\text{Compute}_{\texttt{Glister}} = 3kT\,f_{\text{large}} + \mathcal{O}\left(\frac{\big(kQ + N\log(1/\epsilon)\big)\,f_{\text{large}}\,T}{\gamma}\right)}$$

Selection-stage storage overhead. Storage overhead is from validation caches:

$$\boxed{\text{StorageOverhead}_{\texttt{Glister}} = \mathcal{O}(Q) \quad \text{(validation cache)}}$$

Example scenario values:

$$\begin{aligned}\text{Compute}_{\texttt{Glister}} &\approx \underbrace{280.061}_{3kT\, f_{\text{large}}\ \text{(PFLOPs)}} + \underbrace{60{,}017.420}_{\frac{T}{\gamma}(kQ+N\log(1/\epsilon))\, f_{\text{large}}\ \text{(PFLOPs; } \epsilon=0.01,\ \gamma=20)} \\ &= \mathbf{60{,}297.481}\ \text{PFLOPs},\end{aligned}$$

$$\text{StorageOverhead}_{\texttt{Glister}} \approx Q \times 4 = 51{,}248\ \text{B} \approx \mathbf{5.1 \times 10^{-5}}\ \text{GB}\ (\approx 0.05\ \text{MB}).$$

E.2.3 GraphCut-based Data Subset Selection (`GraphCut`)

`GraphCut` (Iyer et al., 2021) selects $\mathbf{S}_j$ via the generalized graph-cut function

$$f(\mathbf{S}_j) = \lambda \sum_{m \in \mathbf{S}} \sum_{j \in \mathbf{S}_j} s(m, j) \ - \sum_{j_1, j_2 \in \mathbf{S}_j} s(j_1, j_2), \quad \lambda \geq 2.$$

Execution. `GraphCut` *adds* a one-time selection stage prior to training (it does not replace training). The procedure is:

i) train a proxy model;
ii) extract features for all N training points using the trained proxy (per-example cost $f \ll f_{\text{large}}$);
iii) run (stochastic-)greedy selection to build a size-k subset.

(Similarity operations are typically much cheaper than (ii)–(iii), so we absorb them into big-$\mathcal{O}$.)

Overall compute (train-on-coreset). One-time selection (including proxy training) + large-model training:

$$\boxed{\text{Compute}_{\texttt{GraphCut}} = \underbrace{3N\,T_{\text{proxy}}\, f}_{\text{train proxy}} + \underbrace{Nf}_{\text{feature extraction}} + \underbrace{\mathcal{O}(N^2 k)}_{\text{greedy selection}} + \underbrace{3kT\, f_{\text{large}}}_{\text{train large on coreset}}}$$

Selection-stage storage overhead. Storage overhead is from storing pairwise similarities

$$\boxed{\text{StorageOverhead}_{\texttt{GraphCut}} = \mathcal{O}(N^2) \quad \text{(pairwise similarities / kernel)}}$$

Example scenario values:

$$\begin{aligned}\text{Compute}_{\texttt{GraphCut}}\ \text{(PFLOPs only)} &\approx \underbrace{622.663}_{3NT_{\text{proxy}}f} + \underbrace{2.306}_{Nf} + \underbrace{280.061}_{3kT\, f_{\text{large}}} \\ &= \mathbf{905.031}\ \text{PFLOPs},\end{aligned}$$

$$\begin{aligned}\text{StorageOverhead}_{\texttt{GraphCut}}\ \text{(float32)}:\ &\text{full kernel peak} \approx \mathbf{6{,}434.944}\ \text{GB}, \\ &\text{half kernel peak} \approx \mathbf{3{,}217.493}\ \text{GB}.\end{aligned}$$

E.2.4 Reconstructing the Decision Boundary (`BoundarySet-CCS`)

`BoundarySet-CCS` (Yang et al., 2024) selects samples *near the model's decision boundary* and then enforces *coverage* across distance bands. Distance-to-boundary is approximated per sample by the minimum number of PGD steps required to flip its prediction; `CCS` (coverage-centric sampling) then allocates the coreset budget across bands to preserve distribution coverage.

Execution. One-time selection with a proxy, then train the large model on the coreset for all T epochs:

i) *Train proxy:* train a proxy network on all N samples for T_{proxy} epochs (per-example forward cost f, parameters p).
ii) *Distance-to-boundary (PGD):* for each sample, run projected gradient steps until misclassification (cap at $K_{\max}$ steps). If the stopping step is k, define $d(x) = k$. Each PGD step requires one forward & one backward; we use $3f$ per step in our convention. Let $\bar{K} \leq K_{\max}$ be the average steps per sample.
iii) *CCS selection:* partition samples by $d(x) \in \{0, \ldots, K_{\max}\}$ and allocate the size-k budget across bands (linear-time bucketting and sampling).
iv) *Train large on coreset:* train the large model on the selected k points for *all* T epochs.

End-to-end compute (selection + coreset training).

$$\boxed{\text{Compute}_{\texttt{BoundarySet-CCS}} = \underbrace{3N\,T_{\text{proxy}}\,f}_{\text{train proxy}} + \underbrace{3N\,\bar{K}\,f}_{\text{PGD distance-to-boundary sweeps}} + \underbrace{3k\,T\,f_{\text{large}}}_{\text{train large on coreset}}}$$

Selection-stage storage overhead. Storage is mainly through the scalar distance per sample during selection:

$$\boxed{\text{StorageOverhead}_{\texttt{BoundarySet-CCS}} = \mathcal{O}(N) \;\; \text{(per-sample distance)}}$$

Example scenario values (ImageNet-1k; T_{proxy}=90, $K_{\max}$=50 so $\bar{K}$≈50, T=90).

$$\text{Compute}_{\texttt{BoundarySet-CCS}} \text{ (PFLOPs only)} \approx \underbrace{622.663}_{3NT_{\text{proxy}}f} + \underbrace{345.924}_{3N\bar{K}f} + \underbrace{280.061}_{3kT\,f_{\text{large}}} = \mathbf{1{,}248.648} \text{ PFLOPs},$$

$$\text{StorageOverhead}_{\texttt{BoundarySet-CCS}} \text{ (float32)} \approx N \times 4 = \mathbf{0.005} \text{ GB}.$$

E.3 Training Property-based Methods

E.3.1 Samples with Low Loss Curvature (`SloCurv`)

`SloCurv` (Garg & Roy, 2023) scores each training sample by an *input-loss curvature* proxy computed at the end of (proxy) training. For a sample $\vec{z}_m$, with model parameters θ^T and random Rademacher directions v_r scaled by h, the score is

$$\text{Curv}(\vec{z}_m; \theta^T) \;=\; \frac{1}{R} \sum_{r=1}^{R} \left\| \nabla_{\vec{z}} \big[\ell\big(\theta^T, \vec{z}_m + h v_r\big) - \ell\big(\theta^T, \vec{z}_m\big) \big] \right\|_2^2 .$$

Samples with the lowest curvature are retained to form a size-k coreset.

Execution. One-time selection prior to training the large model; *a proxy model is used for scoring*:

i) *Train proxy:* train a proxy encoder with per-example forward FLOPs f and parameters p for T_{proxy} epochs on all N points.
ii) *Curvature scoring:* at the end of proxy training, for each sample compute $\text{Curv}(\vec{z}_m; \theta^T)$ using R Hutchinson repeats. This requires (R+1) gradient evaluations per sample (one at $\vec{z}_m$ and one for each $\vec{z}_m + hv_r$), each costing ≈ (1 fwd + 1 bwd) ≈ $3f$ in our convention.
iii) *Train on coreset:* select the k lowest-curvature samples and train the large model on this coreset for T_{late}=T epochs.

End-to-end compute (selection + coreset training).

$$\boxed{\text{Compute}_{\texttt{SloCurv}} = \underbrace{3N\,T_{\text{proxy}}\,f}_{\text{train proxy}} + \underbrace{3N\,(R{+}1)\,f}_{\text{curvature scoring at end of proxy training}} + \underbrace{3k\,T_{\text{late}}\,f_{\text{large}}}_{\text{train large on coreset}}}$$

Selection-stage storage overhead. Storage overhead is from keeping a track of the running curvature values and the directions probed.

$$\boxed{\text{StorageOverhead}_{\texttt{SloCurv}} = \mathcal{O}(N) \;+\; \mathcal{O}(Rd) \;\; \text{(running stats + } R \text{ probe dirs)}}$$

Example scenario values (ImageNet-1k; T_{proxy}=90, T_{late}=90, R=10).

$$\text{Compute}_{\texttt{SloCurv}}\ (\text{PFLOPs only}) \approx \underbrace{622.663}_{3NT_{\text{proxy}}f} + \underbrace{76.103}_{3N(R+1)f} + \underbrace{280.061}_{3kT_{\text{late}}\,f_{\text{large}}} = \mathbf{978.827}\ \text{PFLOPs},$$

$$\text{StorageOverhead}_{\texttt{SloCurv}}\ (\text{float32}) \approx N \times 4 + Rd \times 4 = 11{,}094{,}540\ \text{B} = \mathbf{0.011}\ \text{GB}.$$

E.3.2 Temporal Dual-Depth Scoring (TDDS)

TDDS (Zhang et al., 2024) builds a coreset by combining two temporal depths of signal from training with a *proxy* model. Depth 1 computes, for each epoch, the projection of each sample's *per-sample gradient* onto the epoch's accumulated gradient direction. Depth 2 then aggregates these per-epoch contributions over a sliding window of length J and emphasizes their *temporal variability* (e.g., windowed variance). We maintain windowed statistics in a streaming manner (constant-time updates), so full trajectories need not be stored.

Execution. One-time selection with a proxy; the large model then trains on the coreset for the full T epochs:

i) *Train proxy:* train a proxy for T_{proxy} epochs on all N samples (per-example forward FLOPs f, parameters p); accumulate the epoch gradient direction.
ii) *Per-sample gradients:* after each proxy epoch, run a scoring sweep to compute per-sample gradients and their projections onto the epoch direction (costing one forward+backward per sample); update the J-length windowed statistics and TDDS score (streaming).
iii) *Select & train large:* rank by TDDS and keep the top-k; train the large model on these k samples for *all* T epochs.

End-to-end compute (selection + coreset training).

$$\boxed{\text{Compute}_{\texttt{TDDS}} = \underbrace{3N\,T_{\text{proxy}}\,f}_{\text{train proxy}} + \underbrace{3N\,T_{\text{proxy}}\,f}_{\text{per-sample gradient sweeps for TDDS}} + \underbrace{3k\,T\,f_{\text{large}}}_{\text{train large on coreset}}}$$

Selection-stage storage overhead. Streaming TDDS requires a J-length buffer of scalar contributions per example (and a temporary epoch-direction vector):

$$\boxed{\text{StorageOverhead}_{\texttt{TDDS}} = \mathcal{O}(NJ)\ \ (\text{windowed logs})}$$

Example scenario values (ImageNet-1k; T=90, T_{proxy}=90, J=10).

$$\text{Compute}_{\texttt{TDDS}}\ (\text{PFLOPs only}) \approx \underbrace{622.663}_{3NT_{\text{proxy}}f} + \underbrace{622.663}_{\text{per-sample gradient sweeps}} + \underbrace{280.061}_{3kT\,f_{\text{large}}} = \mathbf{1{,}525.387}\ \text{PFLOPs},$$

$$\text{StorageOverhead}_{\texttt{TDDS}}\ (\text{float32}) \approx NJ \times 4 = 50{,}734{,}200\ \text{B} = \mathbf{0.051}\ \text{GB}.$$

E.3.3 Using Prediction Uncertainty with a Proxy (Dyn-Unc, DUAL)

Dyn-Unc (He et al., 2024) measures prediction uncertainty via a sliding window of length J over per-example target-class probabilities and averages the windowed uncertainty across proxy training.

DUAL (Cho et al., 2025) combines *uncertainty* with *difficulty* (window-mean prediction) and computes scores from an *early* stage of proxy training.

Execution. One-time selection with a proxy; the large model then trains on the coreset for the full T epochs:

i) *Train proxy:* train a proxy with per-example forward FLOPs f and parameters p for T_{proxy} epochs; maintain sliding-window statistics (length J) via $O(1)$ updates per visit.
ii) *Score & select:*

- `Dyn-Unc`: use windowed uncertainty (variance over the last J predictions), averaged over all proxy epochs T_{proxy}.
- `DUAL`: use the product of windowed uncertainty and difficulty (window mean), averaged over the *early* proxy epochs $T_{\text{proxy,early}} \leq T_{\text{proxy}}$.
- *Beta sampling* (`DUAL`): apply pruning-ratio–adaptive sampling based on a Beta distribution to stabilize extreme pruning. This adds negligible compute and storage.

iii) *Train on coreset (large model):* train for *all* T epochs on the top-k points.

End-to-end compute (selection + coreset training).

$$\boxed{\begin{aligned} \text{Compute}_{\texttt{Dyn-Unc}} &= \underbrace{3N\,T_{\text{proxy}}\,f}_{\text{train proxy + logging}} + \underbrace{3k\,T\,f_{\text{large}}}_{\text{train large on coreset}}, \\ \text{Compute}_{\texttt{DUAL}} &= \underbrace{3N\,T_{\text{proxy,early}}\,f}_{\text{early proxy scoring}} + \underbrace{3k\,T\,f_{\text{large}}}_{\text{train large on coreset}}. \end{aligned}}$$

Selection-stage storage overhead. Only require a scalar window of values per example.

$$\boxed{\begin{aligned} \text{StorageOverhead}_{\texttt{Dyn-Unc}} &= \mathcal{O}(NJ), \\ \text{StorageOverhead}_{\texttt{DUAL}} &= \mathcal{O}(NJ). \end{aligned}}$$

Example scenario values (ImageNet-1k; T=90, T_{proxy}=90, $T_{\text{proxy,early}}$=50, J=10).

$$\text{Compute}_{\texttt{Dyn-Unc}}\ (\text{PFLOPs only}) \approx \underbrace{622.663}_{3NT_{\text{proxy}}f} + \underbrace{280.061}_{3kT\,f_{\text{large}}} = \mathbf{902.724}\ \text{PFLOPs},$$

$$\text{Compute}_{\texttt{DUAL}}(\text{PFLOPs only}) \approx \underbrace{345.924}_{3NT_{\text{proxy,early}}f} + \underbrace{280.061}_{3kT\,f_{\text{large}}} = \mathbf{625.985}\ \text{PFLOPs},$$

$$\text{StorageOverhead (float32)} \approx NJ \times 4 = \mathbf{0.051}\ \text{GB for each.}$$

E.4 Our Method - Correlation of Loss Differences (`CLD`)

`CLD` builds a coreset by leveraging only *loss values* over training: it records the per-epoch losses of all training points and a small held-out query set, then ranks training examples using the correlation of loss *differences* across epochs between train and query. No gradients or Hessians are required.

Execution. One-time selection with a proxy, followed by large-model training:

i) *Train proxy:* train a proxy model for T_{proxy} epochs on all N samples (per-example forward cost f, parameters p).

ii) *Collect losses:* during proxy training, record per-epoch losses for all N training samples (no extra compute beyond the training pass), and run a forward pass on all Q query samples each epoch to record their losses (Qf FLOPs per epoch).

iii) *Score & select:* compute `CLD` scores (correlations of loss differences over epochs) and select a size-k coreset. The arithmetic for correlations/ranking is linear-time in the number of stored losses and is negligible compared to FLOPs above.

iv) *Train on coreset:* train the large model on the selected k points for T epochs.

End-to-end compute (selection + coreset training).

$$\boxed{\text{Compute}_{\texttt{CLD}} = \underbrace{3N\,T_{\text{proxy}}\,f}_{\text{train proxy}} + \underbrace{Q\,T_{\text{proxy}}\,f}_{\text{query loss collection}} + \underbrace{3k\,T\,f_{\text{large}}}_{\text{train large on coreset}} \qquad (\text{FLOPs})}$$

Selection-stage storage overhead. We store loss scalars for all N training and Q query samples across T_{proxy} epochs:

$$\boxed{\text{StorageOverhead}_{\texttt{CLD}} = \mathcal{O}\big((N{+}Q)T_{\text{proxy}}\big) \quad \text{(loss logs)}}$$

Example scenario values (ImageNet-1k; T_{proxy}=90, T=90).

$$\text{Compute}_{\texttt{CLD}} \text{ (PFLOPs only)} \approx \underbrace{622.663}_{3NT_{\text{proxy}}f} + \underbrace{2.097}_{QT_{\text{proxy}}f} + \underbrace{280.061}_{3kT_{\text{late}}f_{\text{large}}} = \mathbf{904.821} \text{ PFLOPs},$$

$$\text{StorageOverhead}_{\texttt{CLD}} \text{ (float32)} \approx (N{+}Q)T_{\text{proxy}} \times 4 = 461{,}220{,}120 \text{ B} = \mathbf{0.461} \text{ GB}.$$

F Comparison of CLD with Influence

The impact measured by CLD closely aligns with the "*influence*" of individual training samples on a model's predictions that are measured by *Training Data Attribution* (TDA) methods. TDA methods have been widely employed for tasks such as debugging datasets, interpreting models, and optimizing training efficiency Koh & Liang (2017); Yeh et al. (2018); Feldman & Zhang (2020).

The earliest TDA methods utilized *Leave-One-Out* (LOO) training, which involves retraining the model after removing specific data points and observing the changes in performance. While straightforward, LOO retraining is computationally prohibitive for modern deep learning models due to the need for multiple retraining cycles Koh & Liang (2017). Recent TDA metrics, such as FZ-Influence (`Infl`) Feldman & Zhang (2020) and `Datamodels` Ilyas et al. (2022), have gained popularity owing to precomputed scores for widely-used datasets in computer vision. These methods, however, face scalability challenges.

A prominent alternative that arose was *Influence Functions*, which estimated the effect of downweighting individual samples using first-order (gradient) and second-order (Hessian) computations Koh & Liang (2017); Basu et al. (2021) performed at the end of training. Methods like `RandSelect` Wojnowicz et al. (2016) and `Arnoldi` iterations Schioppa et al. (2022) improved computational efficiency by approximating the Hessian. Similarly, `TRAK` Park et al. (2023) combined random projections, gradient-based methods, and ensembling to estimate the influence of training samples. However, these approaches often rely on strong assumptions, such as convergence to a unique optimal solution, which limits their applicability to neural networks. Additionally, Hessian computations introduce significant computational overhead. To address these challenges, *unrolling-based* methods that observe the learning process across training iterations have been proposed. These techniques approximate the impact of samples by differentiating through the optimization trajectory Hara et al. (2019). Among these, `TracIn` Pruthi et al. (2020) is a highly efficient method that estimates influence using gradients tracked throughout training. Its practical implementation, `TracInCP`, uses intermediate checkpoints to alleviate computational burdens. While effective, unrolling methods require storing intermediate training states, leading to high storage and computational costs.

In contrast, CLD solely relies on loss trajectories rather than first- or second-order quantities (e.g., gradients and Hessians).

In order to measure the "influence" of a training sample $\vec{z}_m$ on an individual unseen (or query) sample $\vec{z}_q$, we modified Definition 1 slightly to be

$$\texttt{CLD}_{\texttt{infl}}(\vec{z}_m, \vec{z}_q) \coloneqq \rho\left(\vec{\Delta}_m, \vec{\Delta}_q\right) \tag{64}$$

We will now compare the impact measured by this metric ($\texttt{CLD}_{\texttt{infl}}$) to the influence measured by TDA metrics, by utilizing the *linear datamodeling score* (LDS) introduced by Park et al. (2023). LDS measures the correlation between group-level attribution scores ($\texttt{CLD}_{\texttt{infl}}$ or influence) and their observed impact on model predictions when subsets of training data are used.

LDS definition For a query data point z_q, random subsets $\{\mathcal{S}_j\}_{j=1}^{C}$ are sampled from the training dataset, where each subset $\mathcal{S}_j$ contains $\lceil \alpha N \rceil$ points, with $\alpha \in (0, 1)$ as the sampling ratio. Each subset $\mathcal{S}_j$ is used to retrain the model R times with different initializations $\{\xi_r\}_{r=1}^{R}$ and training parameters λ, resulting in

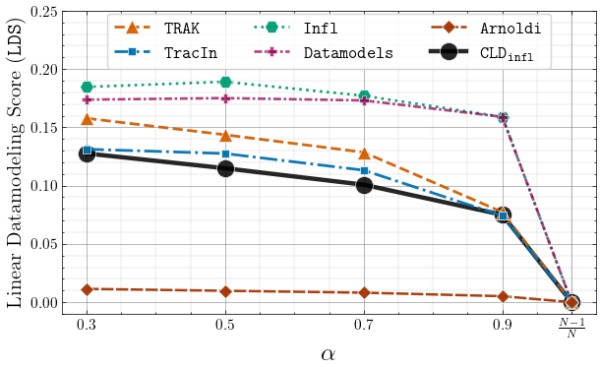

(a) Linear datamodeling scores (LDS) of existing TDA metrics compared to $\texttt{CLD}_{\texttt{infl}}$. The scores were evaluated on CIFAR-10, ResNet-9 with 200 (randomly selected) query samples evaluated over 100 subsets.

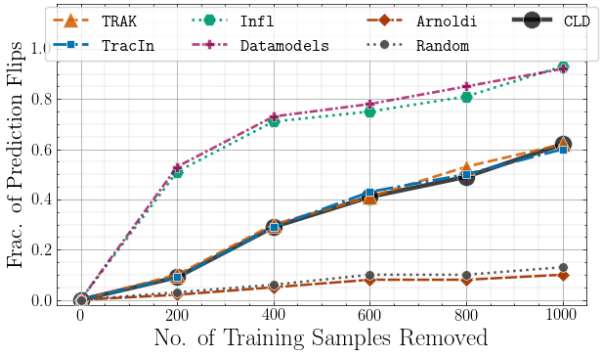

(b) Prediction brittleness of CLD and TDA metrics on CIFAR-10 with ResNet-9. The top-k influential training samples were removed, and the average prediction flips for 200 query samples over 5 seeds are shown.

Figure 8: Comparison of CLD to TDA metrics. (Best viewed in color.)

the model $\theta^T_{S_j,\xi_r}$. This trained model is then used to compute a measurable quantity $f(\vec{z}_q, \theta^T_{S_j,\xi_r})$. A *group attribution score*, $g_\tau(\vec{z}_q, \mathcal{S}_j, \mathcal{S})$, is calculated as $g_\tau(\vec{z}_q, \mathcal{S}_j, \mathcal{S}) \coloneqq \sum_{\vec{z}\in\mathcal{S}_j} \tau(\vec{z}_q, \vec{z}, \mathcal{S})$, where $\tau(\vec{z}_q, \vec{z}, \mathcal{S})$ is the attribution score for a training point $\vec{z}$ with respect to $\vec{z}_q$. The LDS is then obtained using Spearman's rank Spearman (1904) correlation (ρ_s):

$$\texttt{LDS}(\vec{z}_q, \alpha) \coloneqq \rho_s\left(\left\{\frac{1}{R}\sum_{r=1}^{R} f\left(\vec{z}_q, \theta^T_{S_j,\xi_r}\right)\right\}_{j=1}^{C}, \{g_\tau\left(\vec{z}_q, \mathcal{S}_j, \mathcal{S}\right)\}_{j=1}^{C}\right) \tag{65}$$

Experimental Setup: We compared the LDS scores of $\texttt{CLD}_{\texttt{infl}}$ against those of TRAK, Arnoldi, TracIn, Infl, and Datamodels. Precomputed scores for Infl and Datamodels were used for the CIFAR-10 dataset Krizhevsky et al. (2009) with ResNet-9 He et al. (2016), while 10 models were trained for TRAK, Arnoldi, TracIn, and $\texttt{CLD}_{\texttt{infl}}$. The evaluation employed $C = 100$ random subsets, sampling ratios α ranging from 0.3 to $\frac{N-1}{N}$, a query set of 200 samples, and $R = 10$ seeds. The measurable quantity was the accuracy of query samples.

Results and Observations: The results presented in Figure 8a reveal that while the impact captured by $\texttt{CLD}_{\texttt{infl}}$ is distinct from the influence measured by traditional TDA metrics, it aligns closely with methods such as TracIn and TRAK in terms of behavior while being resource-efficient. Notably, the performance gap between these computationally intensive methods and $\texttt{CLD}_{\texttt{infl}}$ narrows as α increases. The drop in LDS scores at $\alpha = \frac{N-1}{N}$ is due to the stochastic nature of model retraining[1].

Takeaways: Although $\texttt{CLD}_{\texttt{infl}}$ (and in essence CLD) fundamentally differs from influence-based TDA metrics, it mirrors their trends at higher sampling ratios while maintaining superior computational efficiency, solidifying its utility as a practical tool for analyzing training dynamics.

F.1 Importance of the Top-k Samples

We demonstrate that the samples identified by CLD are indeed pivotal for generalization, addressing the question: *"Are the training samples with the top-k scores truly the most critical for forming a coreset?"* This is evaluated using the *prediction brittleness* metric. This is also mentioned briefly in Section 8.

Experimental Setup: To quantify the influence of top-k samples, we systematically removed the most impactful data points identified by their CLD scores, from the training set and retrained the model. The metric of interest was the fraction of prediction flips observed in a held-out query set after retraining. If these samples are truly critical for generalization, their removal should cause substantial prediction changes. This experiment also included a comparative analysis with the top-k influential samples identified by TDA

[1]This observation is consistent with the findings of previous research Karthikeyan & Søgaard (2021); Bae et al. (2024).

scores, discussed in this section. Experiments were performed on the CIFAR-10 dataset using a ResNet-9 architecture, with a randomly selected query set of 200 samples. For each configuration, once the top-k samples were excluded, the model was retrained 5 times to account for randomness, and the average fraction of prediction flips was recorded.

Results and Observations: The results, summarized in Figure 8b, illustrate that the top-k samples identified by `CLD` have a comparable influence on prediction outcomes to those identified by TDA-based metrics such as `TracIn` and `TRAK`. Notably, removing the top-800 samples of CIFAR-10, which constitutes just 1.6% of the dataset, results in prediction flips for over half of the query set. This highlights the significant role of the samples identified by `CLD` in supporting model generalization. While metrics like `Datamodels` and `Infl` exhibit greater impact, they are computationally prohibitive, rendering them unsuitable for large-scale coreset generation.

Takeaways: `CLD` emerges as an effective and computationally efficient approach for identifying training samples critical to generalization, making it a practical tool for coreset selection in large-scale machine learning pipelines.